Published in final edited form as:

Nat Biomed Eng. 2020 March ; 4(3): 298–313. doi:10.1038/s41551-020-0528-7.

Selective imaging of solid tumours via the calcium-dependent high-affinity binding of a cyclic octapeptide to phosphorylated Annexin A2

Duanwen Shen[1,&], **Baogang Xu**[1,&], **Kexian Liang**[1], **Rui Tang**[1], **Gail P. Sudlow**[1], **Christopher Egbulefu**[1], **Kevin Guo**[1], **Avik Som**[1,2], **Rebecca Gilson**[1,2], **Dolonchampa Maji**[1,2], **Suman Mondal**[1,2], **LeMoyne Habimana-Griffin**[2], **Walter Akers**[1], **Shunqiang Li**[4], **Yang Liu**[1], **Sharon Bloch**[1], **Sid Kurkure**[1], **Zohar Nussinov**[5], **Alexander Seidel**[5], **Shaw-Wei D. Tsen**[1], **Samuel Achilefu**[1,2,3,4,*]

[1]Department of Radiology, Washington University, St. Louis, MO, 63110, USA

[2]Department of Biomedical Engineering, Washington University, St. Louis, MO, 63110, USA

[3]Department of Biochemistry & Molecular Biophysics, Washington University, St. Louis, MO, 63110, USA

[4]Department of Medicine, Washington University, St. Louis, MO, 63110, USA

[5]Department of Physics, Washington University, St. Louis, MO, 63110, USA

Abstract

The heterogeneity and continuous genetic adaptation of tumours complicate their detection and treatment via the targeting of genetic mutations. However, hallmarks of cancer such as aberrant protein phosphorylation and calcium-mediated cell signalling provide broadly conserved molecular targets. Here, we show that, for a range of solid tumours, a cyclic octapeptide labelled with a near-infrared dye selectively binds to phosphorylated Annexin A2 (pANXA2), with high affinity at high levels of calcium. Because of cancer-cell-induced pANXA2 expression in tumour-associated stromal cells, the octapeptide preferentially binds to the invasive edges of tumours, and then traffics within macrophages to the tumour's necrotic core. As proof-of-concept applications, we used the octapeptide to detect tumour xenografts and metastatic lesions, and to perform fluorescence-guided surgical tumour resection, in mice. Our findings suggest that high levels of pANXA2 in association with elevated calcium are present in the microenvironment of most solid

*Corresponding author, achilefu@wustl.edu.

&These authors contributed equally

Author contributions

S.A. conceived study and designed LS301; D.S., B.X. screened and biologically validated LS301; D.S., B.X., R.T., and S.A. designed the research; D.S., B.X., R.T., K.L., G.P.S., C.E., S.W.D.T., A.S., R.G., D.M., L.H.G., W.A., Y.L., S.B., S.M., S.K., Z.N., K.G., and A.S. performed the research; S.L. developed the breast cancer PDX model; S.A. supervised overall study; S.W.D.T., D.S., B.X., R.T., and S.A. wrote the manuscript. All authors reviewed and edited the manuscript.

Competing interests

S.A. is a co-inventor on a US patent issued to Washington University covering LS301. The patent may become the subject of a licensing agreement in the future. The remaining authors declare no competing interests.

cancers. The octapeptide might be broadly useful for selective tumour imaging and for delivering drugs to the edges and to the core of solid tumours.

Elevated chronic inflammatory milieu, metabolic aberrations, and genetic mutations drive the dynamic adaptation of cancer cells toward their survival, proliferation, and metastasis[1]. Accompanying these neoplastic transformations are alterations in cellular processes that produce heterogeneous populations of cancer subtypes and distorted stroma characterized by diverse cancer biomarkers[2]. Progress in cancer targeted therapies and imaging largely rely on the effectiveness of selectively delivering the enabling molecules to overexpressed cell surface proteins with varying levels of success. Yet, the evolving landscape of tumour survival mechanisms imposes the impossible task of developing a myriad of molecularly targeted drugs and imaging agents for each cancer type.

Numerous studies have shown that neoplastic transformations in solid tumours are accompanied by fundamental changes in cellular signalling processes that are reflected in posttranslational modifications (PTMs) such as phosphorylation, glycosylation, methylation/acetylation, and ubiquitination of proteins resulting in aberrant protein function in the tumour microenvironment (TME)[3]. These cancer-associated PTMs provide an attractive potential source of molecular targets for diagnostic and therapeutic applications, as exemplified by glycosylation-based markers such as CA19-9 and AFP-L3 utilized in modern clinical oncology[4]. Unfortunately, the low abundance of known PTM molecular targets hinders their use as cancer biomarkers[5–8]. Furthermore, most cancer-associated PTMs found to date are confined to few cancer types, and those that are constitutively expressed in most cancer microenvironment are difficult to target selectively[9]. Thus, the full potential of PTM-based molecular targets for imaging and therapy remains to be realized.

Annexin A2 (ANXA2), a member of the annexin family of calcium-dependent phospholipid-binding proteins, is a widely-studied protein known to exhibit cancer-associated PTM[10]. Its upregulation in many cancers including breast, colon, liver, pancreatic, and brain tumours[11,12] suggests a key function in tumour proliferation, angiogenesis, invasion, and metastasis[11,13–17]. Phosphorylation of ANXA2 at tyrosine 23 (pANXA2) modulates ANXA2 tetramer formation and is a prerequisite for its translocation to the plasma membrane[10,18,19]. This PTM occurs in response to growth factor signalling and promotes cancer cell migration and invasion by activating cytoskeletal rearrangements and epithelial-mesenchymal transition[19–22]. Cell surface-associated pANXA2 binds and stabilizes the plasminogen receptor S100A10/p11, which associates with tissue plasminogen activator (tPA) and plasminogen to generate plasmin[10], resulting in enhanced matrix invasion of tumour cells and migration of tumour-promoting macrophages into tumours[23]. Most ANXA2-based drug delivery strategies rely on the overexpression of ANXA2 in certain tumours, but non-tumour tissues also express sufficiently elevated levels to impair selectivity, leading to a requirement for pre-imaging and tissue biopsy to determine the usefulness of the drugs for treating specific tumours.

Here we report that pANXA2 is an inducible hallmark of diverse solid tumour microenvironments, with its expression confined to tumour regions in association with elevated calcium levels in small animal models and primary human cancer tissues. We

discovered that a cyclic octapeptide that emits near-infrared light, LS301, selectively binds to pANXA2 over the non-activated ANXA2, providing a reporter for this PTM. Histopathology of tissue samples from mice administered with LS301 *in vivo* showed that the compound accumulates in pANXA2-positive cancer cells. We further discovered that cancer cells induce pANXA2 expression in tumour-associated fibroblasts and macrophages to stimulate LS301 accumulation in these cells in both the peripheral and core tumour regions. By detecting pANXA2-associated cells in the TME, LS301 serves as a versatile molecule for targeting and delivering drugs to multiple types of solid tumours. The preferential localization of LS301 at the proliferating edge and inner core of solid tumours provides a strategy to define tumour margins and improve the accuracy of cancer resection during surgery, and to treat cancer simultaneously from the periphery and interior core of the tumour.

Results

LS301 internalizes in solid tumour cells via lipid raft facilitated transport

Previously, we reported the serendipitous discovery of a dye-linear hexapeptide conjugate (Cypate-GRDSPK) that internalized in tumours, with its uptake correlating with the metabolic state of the cancer cells[24]. The hydrophobic near-infrared fluorescent dye cypate enhanced internalization of the peptide in tumours, but the retention was transient and depended on the tumour type and metabolic status. Subsequent studies suggested the association of the peptide with β_3 integrin[25]. Utilizing a nature-inspired stabilization strategy[26], we modified the hexapeptide to include two cysteine residues for intramolecular disulphide cyclization. Cypate dye, the peptide, and LS301 (Fig. 1a) were prepared by standard methods[24,27]. Compound identity, purity, and spectroscopic properties were determined as described in the Online Methods section. Cellular, animal, and *ex vivo* tissue distribution of LS301 fluorescence was recorded at 780/830 nm excitation/emission wavelengths (Fig. 1b).

To assess cellular uptake of LS301, we incubated LS301 with lung (A549), breast (MDA-MB-231 and 4T1), and myeloid leukaemia (HL60) cancer cells, or with human normal dermal fibroblast cells as a non-cancer cell control. We observed a time-dependent uptake in solid cancer cell lines A549, MDA-MB-231, and 4T1, reaching a maximum after 12 h, which was maintained over 24 h (Fig. 1c). However, neither the myeloid leukaemia (HL60) nor fibroblast cells retained LS301 over time. Treatment with cypate alone showed only transient retention in all cells, indicating that cypate may support partial internalization but not retention of LS301 in cancer cells (Supplementary Fig. 1). LS301 initially bound to the plasma membrane of cells at early time points, with well-defined clustering in certain sections of the membrane indicative of an association with lipid rafts (Fig. 1d).

Using 4T1 cells, we explored the global mechanism of internalization at early time points (<1 h) by co-treating the cells with amiloride (inhibitor of macropinocytosis), filipin complex (inhibitor of caveolar transport), or chlorpromazine (inhibitor of clathrin-mediated endocytosis) (Supplementary Fig. 2a–b), with further confirmation using the selective clathrin-mediated endocytosis inhibitor Pitstop 2 (Supplementary Fig. 3). The results suggest that LS301 associates with lipid rafts to undergo endocytosis by a clathrin-

dependent pathway. Significant trafficking of LS301 inside cells occurred after 1 h incubation. Following clathrin-mediated endocytosis, LS301 trafficked into early endosomes (co-localization with Rab5) and later to late endosomes (co-localization with Rab7) (Supplementary Fig. 2c–d). At 5 h post incubation, LS301 was primarily found in lysosomes, mitochondria, and peroxisomes, the latter of which represents the probable final destination prior to degradation (Supplementary Fig. 4), with the ratio in these organelles dependent on the time of measurement.

LS301 binds selectively to pANXA2 protein and its cellular uptake is dependent on pANXA2 expression

To identify the molecular target of LS301, we treated luciferase (luc)-expressing 4T1 cells with LS301 and performed sodium dodecyl sulfate polyacrylamide gel electrophoresis (SDS-PAGE) analysis of the cell lysates, resulting in the identification of multiple LS301-associated protein bands via LS301 near-infrared fluorescence (Supplementary Fig. 5a) or via immunoblot with anti-cypate antibody (Supplementary Fig. 5b). LS301 fluorescence detected bands at approximately 28, 37, and 43 kDa, whereas immunoblotting with anti-cypate antibody yielded the 37 kDa and ~67 kDa bands. In addition to serum albumin (67 kDa), proteomic analysis of the 37 kDa band suggested Annexins A1 (ANXA1), A2 (ANXA2), and A3 (ANXA3) as potential LS301-binding partners (Supplementary Dataset; for full methods, see Proteomics section in Methods). The analysis suggested annexin A3 (ANXA3) as the non-enzymatic protein with the highest percentage sequence coverage at 56%, followed by annexin A1 (ANXA1) at 49%, and subsequently annexin A2 (ANXA2) at 31%.

Previous studies have shown that the cypate dye component of LS301 binds reversibly to the hydrophobic pockets of albumin[28,29], which is a source of nitrogen and energy for tumours[30–32]. Albumin binding, however, is not the primary cause of LS301 tumour uptake and retention as cypate alone or cypate formulated with albumin were not retained significantly in tumours *in vivo* over time (Supplementary Fig. 6).

As such, we next focused on understanding the interaction of LS301 with annexin proteins. Using in vitro binding assays with a glutathione S-transferase (GST)-tagged recombinant ANXA21, ANXA2 and ANXA3 proteins, and LS637 (LS301 peptide alone), we identified ANXA2, but not ANXA1 or ANXA3 as the preferred LS301 target (Supplementary Fig. 5c). Immunoprecipitation studies showing pulldown of LS301-ANXA2 protein complexes by anti-LS301 antibody (Fig. 2a), and by gel electrophoresis demonstrated the specific binding of ANXA2 protein with LS301 (Fig. 2b).

We observed that solid cancer cell lines including 4T1 breast carcinoma, A431 epidermoid carcinoma, A549 lung carcinoma, and BxPC-3 human pancreatic cancer show high expression levels of ANXA2 while the HL60 hematologic cancer cell line does not (Supplementary Fig. 7a). ANXA2 is known to exhibit calcium-dependent association with cholesterol-rich lipid rafts at the cell surface[10,19,33]. Consistent with this, our data indicate that LS301 similarly localizes to lipid rafts in the plasma membrane of cells (Fig. 1d), and binds calcium with apparent Kd of 5.67 ± 2.40 nM as determined by microscale thermophoresis (MST); Supplementary Fig. 8). MST determines the binding affinity of

compounds by measuring the migration of molecules in solution under well-defined temperature gradient (for full method, see section on MST in Online Methods)[34–36].

Cell surface localization of ANXA2, which facilitates its targeting by exogenously administered agents such as LS301, is known to be dependent on Tyr23 phosphorylation[10,18,19]. Therefore, we sought to assess the association of LS301 with pANXA2. Using the MST method with purified ANXA2 and pANXA2 proteins (Supplementary Fig. 7b) and LS301, we determined the apparent Kd for LS301 binding to pANXA2, ANXA2, and ANXA3 proteins as 0.075 ± 0.002 nM; 0.389 ± 0.015 nM; and 6.128 ± 0.280 nM, respectively (Fig. 2c), demonstrating the preferential interaction of LS301 with pANXA2. Adapting this method to lysates of 4T1 cells with normalization for ANXA2 concentration showed a Kd for LS301-4T1 cell lysate of 7.45 ± 0.63 nM (Supplementary Fig. 9a). Treatment of cells with insulin is known to stimulate tyrosine-23 phosphorylation of ANXA2 (pANXA2) and translocation of pANXA2 to cell membranes[10,21], resulting in an activated state of ANXA2 in the tumour microenvironment. Insulin-treated 4T1 cells showed increased levels of pANXA2 relative to unstimulated cells, and this effect was suppressed by co-administration of PP2, a Src family kinase inhibitor[37] (Supplementary Fig. 9b). MST analysis of the interaction between LS301 and lysates of insulin-stimulated 4T1 cells showed that LS301 preferentially bound to lysates of pANXA2-expressing cells with an apparent Kd of 0.017 ± 0.004 nM, again demonstrating orders of magnitude preferential binding to pANXA2 over ANXA2 (Supplementary Fig. 9a). Conversely, inhibition of ANXA2 phosphorylation using PP2 significantly increased the apparent Kd to 11.47 ± 1.80 μM, which is close to the binding affinity between LS301 and lysates of HL60 cells lacking ANXA2 expression (apparent Kd 16.55 μM based on total protein; Supplementary Fig. 9a). The affinity data with LS301 and HL60 cell lysates indicate that LS301 could also be binding to another target, albeit with much lower affinity. However, the observed lack of LS301 uptake in HL60 cells suggests that this low-binding target is intracellular.

In agreement with our in vitro binding data, LS301 showed a substantial degree of co-localization with pANXA2 in LS301-treated A549 and 4T1 cells by near-infrared fluorescence microscopy after short-term (1h) incubation (Fig. 2d). To determine whether cellular uptake of LS301 is dependent on ANXA2 expression, we transfected ANXA2-negative HL60 cells with DNA encoding wild-type ANXA2 fused to yellow fluorescent protein (YFP)[38]. Expression of the ANXA2-YFP fusion restored the capability of HL60 cells to internalize LS301, while control (non-transfected) HL60 cells remained unable to uptake LS301 (Fig. 2e). To assess the dependence of cellular LS301 uptake on ANXA2 phosphorylation, we generated cell lines expressing either phosphorylation-permissive or phosphorylation-defective ANXA2 by transfecting HEK 293T cells with DNA encoding either wild-type ANXA2 fused to green fluorescent protein (GFP), or mutant ANXA2 (Tyr to Ala mutation at position 23) fused to GFP, respectively. Cells expressing the wild-type ANXA2 showed substantially increased pANXA2 expression and cellular uptake of LS301 upon stimulation with insulin, while cells expressing mutant ANXA2 (Y23A) continued to show minimal LS301 uptake or pANXA2 expression with insulin stimulation (Fig. 2f). Therefore, phosphorylation of ANXA2 at Tyr23 is a prerequisite for LS301 binding and uptake by these cells.

To confirm the critical role of ANXA2 binding in cellular LS301 uptake, we assessed whether LS301 uptake in cells could be inhibited by co-administration of a fragment of ANXA2, which serves to block binding. Tissue plasminogen activator (tPA) protein, a known binding partner of ANXA2, binds to a site in the N-terminal domain of ANXA2 comprising the amino acid sequence LCKLSL[39]. LS301 and tPA both contain a peptide sequence characterized by an arginine-aspartic acid (RD) motif, as well as the presence of a redox-sensing cysteine residue, suggesting that they both bind to a similar motif on ANXA2. Indeed, a synthetic LCKLSL peptide inhibited the binding and internalization of LS301 in cells (Supplementary Fig. 10). Taken together, these results demonstrate the selective association of LS301 with pANXA2 and provide an approach to selectively interrogate the biology of pANXA2 *in vitro* and *in vivo*.

Intercellular translocation of pANXA2 from cancer cells to fibroblasts enables fibroblasts to internalize LS301

Given that transfection and activation of ANXA2 in constitutively negative cells can facilitate LS301 uptake, we postulated that intercellular transfer of pANXA2 to non-cancer stromal cells such as normal fibroblasts would induce LS301 endocytosis. Fibroblasts are cells that often associate with cancer cells in the TME, and previous studies have shown that cancer cells can transfer ANXA2 to other cells via exosomes[33]. A co-culture of ANXA2-YFP transfected HL60 cells with fibroblasts showed transfer of fluorescent ANXA2 protein from HL60 cells to fibroblasts (Fig. 3a and Supplementary Fig. 11a), with concomitant increase in fibroblast-associated pANXA2 (Supplementary Fig. 11b). Cell microscopy showed that these fibroblasts do not naturally express pANXA2 or retain LS301 (Supplementary Fig. 11c), in contrast to the ANXA2-YFP transfected HL60 cells (Supplementary Fig. 11d). Co-culture of fibroblasts with wild-type (ANXA2-negative) HL60 cells did not induce LS301 internalization in either of the cell types (Fig. 3b). However, addition of LS301 to fibroblasts that were co-cultured with ANXA2-positive GFP-expressing 4T1 cells resulted in LS301 uptake by both the tumour cells and fibroblasts (Fig. 3b) concomitant with the presence of pANXA2 in both cell types. Efficient intracellular transfer of pANXA2 appeared to require cell-cell contact, as we found no evidence of extracellular vesicle involvement (Supplementary Fig. 11e,f). This result sheds light into the mechanism by which cancer cells stimulate stromal cells to possess tumorigenic properties. Furthermore, by increasing the population of pANXA2-positive cells associated with tumour tissue, cancer cells provide an amplification mechanism to enhance the accumulation of LS301 in tumours.

pANXA2 is selectively expressed in the solid tumour microenvironment

Previous studies have shown that ANXA2 expression is upregulated in many solid tumours and could serve as a biomarker for cancer detection[11,12]. As a result, some imaging agents and inhibitors have been developed to target this protein for cancer detection and treatment, respectively. However, ANXA2 is not confined to tumours, but is also expressed in non-tumour tissue (Fig. 4). The variability of ANXA2 expression levels in tumour and non-tumour tissues requires significant upregulation of the biomarker to reliably bind the ligands in the tumour with high selectivity. On the other hand, the inflammatory nature of the TME and the constant reorganization of tumour stroma results in aberrant protein activation,

associated with PTM (phosphorylation) of ANXA2 to generate pANXA2 in the TME, but not in surrounding normal tissue (Fig. 4).

Immunohistochemical staining for pANXA2 in diverse solid tumours including breast (4T1), fibrosarcoma (HT1080), and pancreatic (BxPC-3) cancers showed that ANXA2 is highly activated (phosphorylated) in TME, irrespective of the solid tumour type (Fig. 4a,b and Supplementary Fig. 12). This phenomenon extends to human cancer, where significant pANXA2 expression was observed in cancer tissues from patients with different subtypes of primary breast cancers including ER+ and triple-negative cancers, but not in healthy breast tissue from the same cancer patients (Fig. 4c–e). The broad expression of pANXA2 among different tumour models in mice and in primary human cancers suggests that it could serve as a unifying target for detecting and selectively delivering drugs to diverse tumours with high selectivity. The preceding data suggest that LS301 could serve as a clinically translatable small molecule that preferentially binds pANXA2 over ANXA2.

LS301 selectively accumulates in diverse solid tumour types in vivo

Non-invasive near-infrared fluorescence imaging of tumours and *ex vivo* evaluation of select organs showed substantial LS301 accumulation in multiple tumour types relative to surrounding tissues, with optimal contrast achieved after 24h post-injection (Fig. 5a–g and Supplementary Fig. 13). *Ex vivo* tissue imaging showed consistently high uptake in tumour tissues and variable retention in the excretion organs such as the liver and the kidneys (Fig. 5h,i). In contrast, sham tumours (mice injected subcutaneously with saline) did not show significant accumulation of LS301 (Supplementary Fig. 14).

To test the ability of LS301 to detect tumour in models that mimic the pathophysiology of human cancer, we used the spontaneous MMTV-PyMT mouse model[40,41], whereby mammary gland-specific expression of PyMT under the control of the MMTV promoter/enhancer in transgenic mice (MMTV-PyMT) results in widespread transformation of the mammary epithelium and the development of multifocal mammary adenocarcinomas and metastatic lesions in the lymph nodes and in the lungs. Similar to humans, tumour formation and progression in these mice is characterized by hyperplasia, adenoma/mammary intra-epithelial neoplasia, and early and late carcinoma[40]. Administration of LS301 to these mice led to the identification of all the spontaneous tumours in this model, despite the unpredictability of the location and time of tumour development (Fig. 5g). Furthermore, even in one apparently failed cancer model that has no observable 4T1luc tumours in the region of implantation, LS301 identified positive lymph nodes where the tumour metastasized (Supplementary Fig. 15), which was validated by co-localization of LS301 fluorescence and bioluminescence signal from tumour cells. This finding demonstrates the potential application of LS301 for lymph node staging in breast cancer patients. With a view to clinical translation, we also explored the detection of breast cancer patient-derived xenograft (PDX) models that closely represent the preferred environment of the human tumours, allowing for the *in vivo* growth of the tumour soon after excision from the human donor[42]. Not only did LS301 selectively accumulate in these tumours (Fig. 5c), it was also retained in the lesion for over 96 h (Supplementary Fig. 16). Control experiments with cypate alone (Supplementary Fig. 6) or with a scrambled LS301 peptide analogue, Cypate-

Cyclo(Cys-Arg-Gly-Asp-Ser-Pro-Cys)-Lys-OH (Supplementary Fig. 17) did not show substantial retention in the tumours. These results demonstrate that LS301 accumulates in a wide range of solid tumours, regardless of tumour type or tissue of origin.

The multifocal distribution of LS301 in tumours correlates with calcium and phosphorylated ANXA2

Given that gross images showed high LS301 fluorescence in tumours, we examined the distribution of the molecular probe in frozen tumour sections. In the 4T1 and HT-29 tumour models, the data revealed an excellent correlation of LS301 fluorescence with calcium and pANXA2 expression (Fig. 6a). To characterize the spatial distribution of LS301 in tumours, we sectioned tumours from mice bearing stably transfected 4T1 luc-GFP breast tumours, HT1080 fibrosarcoma tumours, or BxPC-3 pancreatic tumours. We found a bimodal distribution of LS301 with accumulation of LS301 on the proliferating and invasive edges of the tumour as well as in necrotic-appearing regions of the tumour at 24 h post-administration (Fig. 6b–f). In the 4T1 luc-GFP model, flow cytometric analysis of the dissociated tumour tissue showed that at 24h post-LS301 injection, approximately 53.3% of the LS301 fluorescence was associated with GFP-positive tumour cells (Supplementary Fig. 18), with the remaining LS301 fluorescence arising from tumour-associated stromal cells, likely fibroblasts at the tumour margins and tumour-associated macrophages. Intracellular localization of LS301 in 4T1 luc-GFP tumour sections was evidenced by Z-stack imaging (Supplementary Fig. 19). Immunohistochemistry (IHC) analysis for M1 and M2 macrophage populations in sections from 4T1-luc, A431, and DBT tumours revealed a strong co-localization between macrophages and LS301 fluorescence (Supplementary Fig. 20). It is likely that the macrophages phagocytosed LS301-positive cells in the tumour boundaries before migrating to the necrotic region. Some of the macrophages are trapped in transit at the point of imaging. The exact implication of the association of different macrophages with LS301-positive cancer cells is unclear at this time. When LS301 fluorescence in the tumour periphery is high, the signal appears dim inside the tumour. Using fluorescence densitometry, we show an excellent spread of LS301 fluorescence in 4T1, HT1080, and BxCP-3 tumour tissues, irrespective of the tumour type (Supplementary Figure 21).

Our results indicate that the cancer cell-mediated stimulation of pANXA2 expression in associated stromal cells allows LS301 to identify transformed non-tumour cells such as fibroblasts and macrophages that promote tumour growth. This process also allows for the accurate detection of the invading frontiers of tumours, where pANXA2 expression is high. Furthermore, solid tumours typically have positive interstitial pressure that confines drugs and imaging agents to the periphery. Through macrophage-facilitated transport, LS301 can overcome this challenge by delivering drugs both to the invading edges of tumours and to multiple necrotic regions of tumours against a pressure gradient.

We further explored the application of LS301 to fluorescence guided cancer surgery. Real-time assessment of surgical margin is an exciting application of optical imaging methods, a process facilitated by the accumulation of LS301 at the invading boundaries of tumours. Imaging of a subcutaneous model of 4T1luc breast cancer in mice demonstrates the ease of

visualizing LS301 fluorescence in tumours with a head-mounted cancer-viewing device, Cancer Vision Goggles [51,52] (Fig. 7). The method allowed us to visualize and resect the tumours, as well as survey the surgical bed for the presence of any residual cancer (Supplementary Fig. 22).

Discussion

Previous reports have shown that some tumours overexpress ANXA2, leading to the development of some inhibitors and molecular probes for treating and imaging ANXA2-overexpressing tumours. However, this protein is also expressed at high levels in surrounding non-tumour tissue. As a result, the effectiveness of the intervention relies on the higher expression level of ANXA2 in tumour cells compared to neighbouring tissue. We have identified pANXA2 as a universal molecular marker for most solid cancers, one that uniquely arises from cancer-associated phosphorylation events. Such targets exploit the derangements in cellular signaling pathways characteristic to cancer, and provide a significant selectivity advantage over cancer markers based solely on overexpressed proteins. The nature of phosphoprotein targets also enables further enhancement in targeting efficacy through phosphorylation induction strategies. An important function of pANXA2 is to facilitate cancer metastasis and invasiveness, which predominantly occurs at the boundaries and proliferating regions of tumours[19,20,22]. We discovered that LS301 selectively targets pANXA2 in diverse tumours. In small tumours (<5 mm), LS301 coverage is about 100%. However, it accumulates preferentially in the periphery of advanced tumours, where its biodistribution correlates with pANXA2 and calcium expression. In capsular tumours such as breast cancer, the intense LS301 fluorescence arose from both tumour cells and cancer-associated fibroblasts.

LS301 does not bind to non-tumour-associated fibroblasts, indicating that the tumour-associated fibroblasts could express pANXA2, which was confirmed by IHC. The ANXA2 levels in the ANXA2-transfected HL60 did not exceed that of naturally expressed ANXA2 in 4T1 breast carcinoma cells (Supplementary Fig. 23), suggesting that the observed ANXA2 transfer between ANXA2-transfected HL60 and fibroblasts was less likely caused by overload of the transfected gene. Our cell studies suggest that there may be a mechanism by which tumour cells upregulate pANXA2 in surrounding fibroblasts via membrane fusion, tunnelling nanotubes, and/or secreted soluble factors. This upregulation is probably mediated through cell-cell interactions because we did not observe evidence of pANXA2 transfer via extracellular vesicles (Supplementary Fig. 11e,f). Co-cultured fibroblasts with HL60-Y showed translocation of ANXA2 to the fibroblasts as early as 4 hours of incubation, a process that increased with time (Supplementary Fig. 11a). To provide evidence that this phenomenon is not limited to myeloid-derived HL60 cells (where ANXA2 transfer could occur through cell fusion or phagocytosis), we demonstrated that co-incubation of 4T1-luc/GFP cells with fibroblasts also induced pANXA2 expression in the fibroblasts (Fig. 3b). Because of the important roles tumour-associated fibroblasts play in harbouring therapy-resistant cancer stem cells, the stimulated uptake of LS301 provides a mechanism to identify the location of these cells and report treatment response. Translocation of ANXA2 to the nucleus of non-cancer cells may contribute to chromosomal instability[43]. Over time, these “compromised” fibroblasts may progress toward a cancer-associated fibroblast state with

associated tumour growth promoting features such as secretion of growth factors and cytokines [44]. Although conventional histopathology focuses on cancer cells, these compromised cells could facilitate the reactivation of dormant cancer cells and subsequent cancer relapse.

We also observed that LS301 binds calcium (Supplementary Fig. 8) and that the addition of calcium in the LS301 formulation increased cellular uptake of the probe *in vitro* (Supplementary Fig. 24) and accelerated its accumulation in tumour tissues *in vivo* (Supplementary Fig. 25). Previous studies have shown that calcium-binding proteins such as the S100 bind to annexins in a calcium-dependent association with lipid rafts[10,45]. Upon binding to calcium, both S100 proteins and annexins undergo structural rearrangement that exposes the hydrophobic sites to enhance binding to other proteins and cell membranes. Although a definite mechanism of how calcium-bound LS301 interacts with pANXA2 remains to be solved, we postulate that LS301 uses a similar mechanism to render the molecule more hydrophobic for facilitated interaction with pANXA2 in calcium-rich environment. For interactions of LS301 with its targets, observable binding occurred *in vitro* in the presence of up to 4% SDS; higher levels of SDS led to dissociation (Supplementary Fig. 26), providing additional support for the high binding affinities we observed. This report focused on the interaction of LS301 with ANXA2 and pANXA2 but it is likely that the agent binds to other biomolecules that were not explored at this time.

The hydrophobic nature of LS301 led us to formulate the compound in PBS containing 1% albumin. This strategy has been used to formulate other drugs such as paclitaxel to form the protein-bound chemotherapeutic Abraxane[46,47]. A mechanism suggested for the improved uptake of Abraxane in tumours is that cancer cells utilize albumin as an energy source and express cell surface receptors such as secreted protein acidic and rich in cysteine (SPARC) that internalize the complex[46,48,49]. Formulation of LS301 with albumin (of human, murine, or canine origin) may create a secondary internalization pathway via the GP60 receptor[50] but this pathway may have limited effect in vivo because formulation of albumin with cypate alone did not induce selective uptake in tumours *in vivo* (Supplementary Fig. 6b).

Postulating that the selective accumulation of LS301 in tumours LS301 could represent a useful vehicle for targeted delivery of drugs to tumours, we conjugated doxorubicin to the free carboxylic acid group of cypate (Supplementary Fig. 27a). Administration of the conjugate into HT1080 tumour-bearing mice led to significant tumour growth suppression and extended survival of mice compared to equivalent dose of the free drug and untreated controls (Supplementary Fig. 27b,c). Unlike the free drug, LS301 does not accumulate in the heart, thus avoiding the dose limiting toxicity of doxorubicin. Further toxicity studies showed no significant effects of LS301 on cell viability *in vitro* at the imaging doses employed (Supplementary Fig. 28).

Our work provides rationale for the development of clinical agents targeting pANXA2. Although monoclonal antibodies remains a mainstay of targeted therapies[53,54], their large size (~150 kDa) limits tumour penetrance and the high production cost confines their use to few clinical centres. Small peptide-based agents such as LS301, which can be synthesized inexpensively at a large scale, represent an advantageous next-generation diagnostic and

therapeutic modality. Efforts are currently underway to assess the efficacy of our low-molecular-weight probes targeting pANXA2 for clinical imaging and drug delivery applications. We envision that successful advancement of these agents will pave the way for expansion of the currently limited repertoire of PTM-based targets in cancer management.

Methods

Chemicals

All the fluorenylmethyloxycarbonyl (Fmoc) amino acids, Wang resin Fmoc-Tyr(tBu)-Wang resin and Fmoc-Lys(Boc)-Wang Resin were purchased from AAPPTec (Louisville, KY, USA). Dichloromethane (DCM), acetic acid, acetic anhydride, phenol, hydroxybenzotriazole (HOBt), N,N-diisopropylethylamine (DIEA), N-trityl-1,2-ethanediamine, phenol, thioanisol, dimethylformamide (DMF), N,N'-diisopropylcarbodiimide (DIC), trifluoroacetic acid (TFA), iodine, methyl tert-butyl ether (MTBE) and O-(7-azabenzotriazol-1-yl)-N,N,N',N'-tetramethyluronium hexafluorophosphate (HATU) were purchased from Sigma-Aldrich (St. Louis, MO, USA). For a full list of chemicals used and their details, please refer to Supplementary Table 1. Water was obtained from a Millipore Q3 system. Lysotracker, BODIPY TR Ceramide, CellLight Peroxisome-GFP, BacMam 2.0, and Fluo-4 calcium probe were purchased from Thermo Fisher Scientific (Waltham, MA). Chlorpromazine hydrochloride, filipin complex, and amiloride hydrochloride were purchased from Sigma-Aldrich (St Louis, MO, USA). Reagents for organelle staining included VectaCell Rhodamine 123 (Vector Laboratories, Burlingame, CA, USA).

Recombinant proteins and antibodies

Recombinant annexin A2, annexin A2 with glutathione-S-transferase (GST) tag (Cat. No.: MBS717197), annexin A1 (Cat. No.: MBS954685), and annexin A3 (Cat. No.: MBS143632) proteins were purchased from MyBioSource, Inc. (San Diego, CA, USA). Purified ANXA2 protein and purified pANXA2 protein were obtained as a gift from Dr. Gabriel Birrane (Beth Israel Deaconess Medical Center, Boston, MA). Rabbit monoclonal anti-annexin A2 antibody (Cat. No.: 8235S) was purchased from Cell Signaling Technology, Inc. (Danvers, MA, USA). Mouse monoclonal anti-β-actin 2A3 (Cat. No.: sc-517582) and mouse monoclonal anti-pANXA2 antibody (11.Tyr 24) (Cat. No.: sc-135752) were purchased from Santa Cruz Biotechnology, Inc. (Dallas, TX, USA). Rabbit polyclonal anti-pANXA2 (phosphor-Tyr24, Cat. No.: MBS9429113) antibody was purchased from MyBioSource, Inc. (San Diego, CA, USA). Rabbit monoclonal anti-Rab5 (C8B1, Cat. No.: 3547) and rabbit monoclonal anti-Rab7 (D95F2, Cat. No.: 9367) primary antibodies were from Cell Signaling Technology (Danvers, MA, USA). Rabbit polyclonal anti-NOS2 (C-19, Cat. No.: sc-649) and rabbit polyclonal anti-ARG1 (H-52, Cat. No.: sc-20150) antibodies were purchased from Santa Cruz Biotechnology (Dallas, TX, USA). Rabbit polyclonal anti-LS301 antibody was generated by Antibody Research Corporation (St Charles, MO, USA) via immunization of New Zealand rabbits with keyhole limpet haemocyanin (KLH)-conjugated LS301 followed by antigen affinity purification of rabbit immunoglobulins from blood; antibody titer was tested by ELISA. Protein A/G agarose (Cat. No.: sc-2003) was purchased from Santa Cruz Biotechnology (Dallas, TX, USA). Tyr24-phosphorylated

ANXA2 protein (pANXA2) was a generated via *in vitro* phosphorylation by overnight incubation of recombinant ANXA2 protein with recombinant ephrin B1 (kinase) and ATP in buffer as previously described[51]. The Vybrant Alexa Fluor 488 lipid raft labelling kit was purchased from Thermo Fisher Scientific (Waltham, MA, USA). For a complete list of antibodies used and their details, please refer to Supplementary Table 2.

Plasmids

Human Anxa2 cDNA subcloned into the pCMV6-AC-GFP vector was purchased from OriGene Technologies (Rockville, MD, USA). cDNA for the mutant pEZ-M98-GFP-Anxa2-Y23A (tyrosine replaced by alanine) was obtained from GeneCopoeia (Rockville, MD, USA). The recombinant plasmids were characterized by restriction digest, and the quality of the expressed recombinant protein was assessed by confocal microscopy for fluorescence integrity and by western blot.

Cell lines and culture

The cancer cell lines 4T1, Lewis Lung Carcinoma (LLC), A431, A549, MDA-MB-231, BxPC-3, and HL-60 were purchased from the American Type Culture Collection (ATCC, Manassas, VA, USA). The 4T1-luciferase (4T1-luc) cell line was obtained as a gift from Dr. Katherine Weilbaecher (Washington University School of Medicine, St Louis, MO, USA). Human dermal fibroblasts were obtained from Coriell Cell Technologies (Camden, NJ, USA). Unless otherwise indicated, all cell lines were cultured at 37°C in 5% CO_2 incubator in appropriate media supplemented with 10% FBS. For a complete list of cell lines and cell culture reagents used, please refer to Supplementary Table 3.

Animals

Five to seven-week old nude (athymic NCr-nu/nu, Cat #555), Balb/c (Cat #553), C57BL/6 (NCl C57BL/6NCr, Cat # 556), or Fox-Chase SCID Beige (Cat # 250) mice were purchased from Charles River Laboratories (Wilmington, MA). WHIM (Washington University Human in Mouse) PDX mice were obtained from the Washington University Institute of Clinical and Translational Sciences, HAMLET (Human and Mouse Linked Evaluation of Tumours) core. MMTV-PyMT mice (Cat #002374-FVB/N-Tg) mice were purchased from Jackson Labs (Bar Harbor, ME). Mice of both genders were used in experiments, with typical age 7-12 weeks (typical weight at these ages 20-30 g) at time of use. All mice were housed in designated animal facilities, fed *ad libitum* and inspected regularly. All animal studies were approved by the Washington University School of Medicine Animal Studies Committee (protocol numbers 20130207 and 20160207) and performed in accordance with humane care and use of research animals.

Human tissues

De-identified human breast tissue sections including malignant triple-negative (n=4) and ER-positive (n=4) and control normal tissues (n= 3) from the breast cancer patients were obtained from the Tissue Procurement Core (TPC) – Siteman Cancer Center and Pathology and Immunology at Washington University School of Medicine (St Louis, MO, USA) in

accordance with Washington University's Institutional Review Board; associated IRB #201906098.

Synthesis of LS301

LS301 (cypate-cyclic ([D]Cys-Gly-Arg-Asp-Ser-Pro-Cys)-Lys-OH) was synthesized as previously reported[52]. Briefly, the linear GRD peptide, H-[D]Cys(Acm)-Gly-Arg(Pbf)-Asp(tBu)-Ser(tBu)-Pro-Cys(Acm)-Lys(Boc)-OH, was prepared via a CEM Liberty Blue microwave peptide synthesizer (Matthews, NC, USA) on the Fmoc-Lys(Boc)-wang resin. The resin (0.1 mmol) was swelled in DCM for 1 h before use. Fmoc-amino acids (0.5 mmol, 5 eq), coupling reagent (HBTU, 0.5 mmol, 5 eq) and DIEA (1 mmol, 10 eq) were added to the resin and the mixture was reacted for 15 min under microwave irradiation (100W, 90°C). The resin was washed three times with DMF. De-protection of Fmoc group was carried out by treatment of 20% piperidine/DMF for 5 min under microwave irradiation (100W, 90°C). The peptidyl resin was washed and the peptide cyclized through the disulfide bridge with iodine (1.2 eq) in DMF for 90 min. Subsequently, cypate (3 eq) was conjugated to the cyclic peptide on solid support in the presence of DIC (5 eq) in DMF to afford the LS301 peptidyl resin. The resin was then treated with a cleavage cocktail of TFA: thioanisol: phenol: water (85:5:5:5, v/v/v/v) for 90 min at room temperature. The cleaved peptide product was concentrated *in vacuo* before performing reverse-phase HPLC purification (Gilson, Middleton, WI, USA). The molecular weight of the final product (1469 Da) was confirmed by electrospray ionization mass spectrometry with peaks observed at 1470 (M+1) and 735 (M+2/2).

Synthesis of LS301 peptide (LS637)

LS637 (Ac-Cyclo([D]Cys-Gly-Arg-Asp-Ser-Pro-Cys)-Lys-OH), a non-fluorescent analogue of LS301, was synthesized by similar method as LS301, except acetic anhydride was used in place of cypate. The molecular weight of the final product (904 Da) was confirmed by electrospray ionization mass spectrometry with peaks observed at 905 (M+1) and 453 (M +2/2).

Synthesis of ANXA2 blocking (LCKLSL) and scrambled (LGKLSL) peptides

AnXA2 binding and scrambled peptides, LCKLSL and LGKLSL, respectively, were synthesized on solid support by standard automated Fmoc chemistry at room temperature. Starting with the rink amide resin (30 μmol), subsequent amino acids were coupled to the resin by using the appropriate Fmoc-protected amino acids (90 μmol) and coupling reagent HBTU (90 μmol), HOBT (90 μmol) and DIEA (180 μmol). Cleavage of the peptide from the resin and concomitant removal of all protecting groups was achieved with 95% TFA, and 5% water. The resulting product was purified by preparative HPLC suing a Grace Vydac C-18 column (250 × 21.2 mm) with UV detector at 254 nm. The desired compound was obtained by linear gradient elution consisting of solvents A (0.1% TFA in water) and B (0.1% TFA in acetonitrile) from 90 % to 10 % over 30 min at 10 mL/min. The purity of the peptide was characterized by analytical HPLC and the identity was confirmed by electrospray mass spectrometry (ES+MS): LCKLSL, calculated m/w 676, observed m/z 677 (M+1); LGKLSL calculated 629.80, observed m/z 629 (M+1).

Synthesis of KLH-conjugated LS301 for antibody production

Synthesis of KLH-conjugated LS301 was accomplished via conjugation of linker to LS301 followed by conjugation of LS301-linker to KLH. For linker conjugation, 180 μmol (34.5 mg) EDC·HCl, 90 μmol (41mg) S-Trityl-L-cystine tert-butyl ester hydrochloride (Chem-Impex, Wood Dale, IL, USA) and 180 μmol (31.2 μl) DIEA in 2 ml DMF was sonicated until a clear solution was obtained. The mixture was added to 30 μmol LS301 and mixed overnight before the resin was filtered and washed with DMF and DCM. Finally, the product was cleaved from the resin and purified by reverse phase HPLC. About 3 mg of the product was obtained (MW: 1572).

Synthesis of LS301-doxorubicin conjugate (LS766)

Doxorubicin (3 eq, LC Laboratories, Woburn, MA) was added to a mixture of The LS301 peptidyl resin, HATU (6 eq) and DIEA (6 eq) in DMF. After 12 h reaction, the resin was treated with a cleavage cocktail consisting of TFA: thioanisol: phenol: water (85:5:5:5, v/v/v/v) for 90 min at room temperature. The cleaved peptide product was concentrated in *vacuo*, then purified on reverse-phase HPLC (Gilson, Middleton, WI, USA) to obtain LS766 (doxorubicin-cypate-cyclic(DCys-Gly-Arg-Asp-Ser-Pro-Cys)-Lys-OH), M/W 1995, ESI-MS observed 998 (M+2/2) and 666 (M+3/3).

Immunoprecipitation studies

In general, immunoprecipitation experiments were performed by incubation of LS301 with either 4T1 cell lysates or live 4T1 cells, followed by pulldown of LS301-associated proteins with anti-LS301 antibody and protein A/G agarose beads.

For cell lysis, whole 4T1 cells were homogenized in a 15ml tube on homogenizer using 3 ml of homogenizing RIPA buffer (10 mM Tris-HCl pH 8.0, 140m M NaCl, 1mM EDTA, 0.5mM EGTA, 1% Triton X-100, 0.1% sodium deoxycholate, 0.1% SDS, 1 mM PMSF, protease inhibitor cocktail (10 μL/mL, Sigma, Cat No.: P8340), and phosphatase inhibitor cocktail 3 (10 μL/mL, Sigma, Cat No.: P0044). Lysates were clarified by centrifugation at 15,000 x g. The concentration of the protein was determined by BAC protein assay (Bio-Rad) with bovine serum albumin (BSA) as a standard. The supernatants were stored at −80°C.

For immunoprecipitation studies with cell lysates, 400μg of cellular protein extract was incubated with LS301 (at a concentration of 40 μM) in 0.5ml 1 X PBS for 2 hrs at room temperature. For immunoprecipitation studies with live cells, 4T1 cells in a T-75 flask at approximately 80% confluence were incubated with LS301 (at a concentration of 10 μM) for 24 h at 37°C; the cells were rinsed with PBS, harvested using trypsin-EDTA, and lysed as above. Next, 10μg of anti-LS301 polyclonal Ab (Antibody Research Corp., St Charles, MO) was added to the sample and incubated for 18 hours at 4°C. 40μl of protein A/G PLUS-agarose beads (Cat. No.: sc-2003, Santa Cruz Biotechnology) was then added, followed by overnight incubation at 4°C under rotation. The pellets were collected by centrifugation (1200 x g) and washed three times with 1 X PBS for 5 min. The pellets were re-suspended in 60μl of 1 x electrophoresis loading buffer containing SDS. Samples were boiled for 7 min. Then 30μl of the samples was resolved on TGX gels (Any Size gradient TGX gels, Cat. No.:

4569034, Bio-Rad) and visualized by near-infrared fluorescence imaging using the Pearl Imaging System, subjected to Bio-Safe Coomassie stain (Cat. No.: 1610786, Bio-Rad), or subjected to Western blot analysis as detailed in Western blot section of Online Methods.

Fluorescent gel binding studies

For fluorescent gel binding experiments, 1 μg recombinant annexin A2 protein was incubated with LS301 or cypate (10 μM) at 37°C for the time periods indicated. Samples were subjected to 12% TGX gels (Cat. No.: 4561044, Bio-Rad, Hercules, CA) and gels were imaged for near-infrared fluorescence (800 nm) using a Pearl Small Animal Imager (LI-COR Biosciences, Lincoln, NE, USA). For competitive binding experiments, Annexin A2-GST, annexin A1, or annexin A3 (1.0 μg protein per sample) was pre-incubated in the presence or absence of 2.5 mM of LS637 (non-fluorescent LS301 analog; blocking peptide) in binding buffer (25 mM Tris-HCl pH 7.4, 150 mM NaCl, 1 mM $MgCl_2$, 1 mM $CaCl_2$) for 1 h at 37°C. 10 μM LS301 was then added to each sample. After incubation for 2 h at 37°C, proteins were subjected to SDS-PAGE and fluorescent imaging as described above. For some experiments, LS301 was incubated with 4T1 tumour cells prior to SDS-PAGE as indicated in the figure legends.

Microscale thermophoresis (MST)

Microscale thermophoresis (MST) is a technique for the study of biomolecular interactions in an aqueous environment in which no immobilization of either reaction partner is required[53]. MST exploits the directed movement of molecules along a microscopic temperature gradient. The rate and direction of movement is dependent upon the size, charge, and solvation shell of the species under study. Any changes in this environment have the potential to change the thermophoretic movement of the species[54]. This technique has been shown to be capable of distinguishing very small changes to protein surfaces that occur, for example, when a small fluorescent molecule binds to the surface of a protein[55,56,57].

MST was performed using the Monolith NT.115 (Nanotemper Technologies, Munchen, Germany). The appropriate agent(s) and LS301 stock samples were denatured in MST-1 buffer (50 mM Tris-HCl, pH 7.4; 150 mM NaCl; 10 mM $MgCl_2$; 2% DMSO; 0.1% Tween-20; 4% SDS, 4 mM DTT) at 97°C for 10 min. Fluorescence was assessed in MST-2 buffer (50 mM Tris-HCl, pH 7.4; 150 mM NaCl; 10 mM $MgCl_2$). The protein was prepared in MST-2 buffer and 20 μL serial dilutions were made with protein concentration ranging from 3.05 pM to 50 nM (pANXA2) or 3.81 pM to 62.5 nM (ANXA2). All samples were loaded into NT.115 standard capillaries. Analysis was performed at 37°C, 30% LED power, 60% MST power and a constant LS301 concentration of 20 nM. The apparent Kd values were calculated from fragment concentration-dependent changes in normalized fluorescence (Fraction Bound) of LS301 after 5 s of thermophoresis based on the law of mass action using the MO Affinity Analysis v2.3 software.

Western blot

Cells were homogenized using an ultrasonic processor in RIPA buffer (10 mM Tris-HCl, pH8.0; 140 mM NaCl; 1 mM EDTA; 0.5mM EGTA; 1% Triton X-100; 0.1% Sodium

deoxycholate; 0.1% SDS; 1 mM PMSF). Total cell lysates were clarified by centrifugation. Total cellular protein or pure proteins were denatured in SDS gel-loading buffer (100 mM Tris-HCl, 200 mM DTT, 4% SDS, 0.2% bromophenol blue, and 20% glycerol) for 7 min at 100°C and then separated on 12% TGX gel (Bio-Rad, Hercules, CA, USA). After electrophoresis, proteins were transferred to PVDF-FL membrane using an EC140 Mini Blot Module (Thermo EC, Holbrook, NY, USA) apparatus. The membrane washttps://www.licor.com/bio/products/reagents/blocking_buffers/odyssey_blocker_pbs.html treated with Odyssey blocking buffer for 1 h at room temperature, followed by incubation with rabbit monoclonal anti-annexin A2 (D11G2, Cell Signaling Technology, Inc.) and mouse monoclonal p-annexin II (11.Tyr24; Santa Cruz Biotechnology) or rabbit Anxa2 (Phospho-Tyr24; MyBioSource, Inc.) primary antibodies in Odyssey blocking buffer at 4°C overnight. After washing three times for 10 min each in PBS with 0.1% Tween-20 (PBS-T), the membrane was incubated for 1 h with diluted IRDye 680RD goat anti-rabbit IgG or IRDye 800CW goat anti-mouse IgG in Odyssey blocking buffer. The membrane was then washed three times for 10 min each in PBS-T and imaging using the Odyssey CLx imaging system. The membrane was re-probed with mouse monoclonal anti-β-Actin (Santa Cruz Biotech) or rabbit polyclonal anti-β-Actin (Cell Signaling Technology) for immunoblotting and imaging. In some experiments Bio-Safe Coomassie stain was used (Bio-Rad, Hercules, CA, USA).

Proteomics

For mass spectrometric protein identification, the appropriate bands were excised from protein gels and submitted for LC-MS/MS protein identification at the Donald Danforth Plant Science Center, Proteomics & Mass Spectrometry Facility (St Louis, MO, USA). Samples were trypsin digested and run on the LTQ-Orbitrap Velos using the 1 h LC-MS/MS method. All MS/MS samples were analyzed using Mascot (Matrix Science, London, UK; version 2.4.1). Mascot was set up to search the cRAP_20110301 database and NCBInr database (selected for Mus musculus, 174101 entries) assuming the digestion enzyme trypsin. Mascot was searched with a fragment ion mass tolerance of 0.80 Da and a parent ion tolerance of 15 PPM. De-amidated of asparagine and glutamine, oxidation of methionine and carbamidomethyl of cysteine were specified in Mascot as variable modifications.

Scaffold (version Scaffold_4.3.4, Proteome Software Inc., Portland, OR, USA) was used to validate MS/MS based peptide and protein identifications. Peptide identifications were accepted if they could be established at greater than 80.0% probability by the Scaffold Local FDR algorithm. Protein identifications were accepted if they could be established at greater than 99.0% probability and contained at least 2 identified peptides. Protein probabilities were assigned by the Protein Prophet algorithm (Nesvizhskii, Al et al Anal. Chem. 2003; 75(17):4646-58). Proteins that contained similar peptides and could not be differentiated based on MS/MS analysis alone were grouped to satisfy the principles of parsimony. Proteins sharing significant peptide evidence were grouped into clusters.

Cellular uptake studies

In general, cultured cancer cells were grown and incubated with the indicated amount of probe in Lab-Tek 8-chambered slides for the indicated time durations. At selected time

points cells were washed with PBS and underwent conventional slide preparation, ICC if indicated, and viewing under epifluorescence or confocal microscopy as described in the Fluorescent Microscopy methods section.

For live cell imaging of LS301 internalization at 37ºC in human dermal fibroblasts (Cat. No.: GM05399, Coriell Institute for Medical Research, Camden, NJ) and tumour cells including 4T1luc, MDA-MB-231 (ATCC, HTB-26), 5TGM, A549 (ATCC, CCL-185) and HL60 (ATCC, CCL-240), cells were cultured in appropriate mediums supplemented with 10% FBS and penicillin/streptomycin and incubated at 37°C in 5% CO2 incubator. The cells were grown on Lab-Tek 8-chamber slides (Nunc Inc. Rochester, NY) in the culture medium overnight prior to the experiment. The compounds were dissolved in 20% DMSO in 10 μM PBS (pH 7.4) (Sigma, St. Louis, MO) for stocking solution and mixed with culture medium to reach the final concentration. Cells were incubated with 1 μM compounds in chamber slides at different time points at 37ºC. After LS301 treatment the culture media was removed and followed by addition of culture media containing SYTO 13 nuclear dye from (Cat. No.: S7575, Thermo Fisher Scientific, Waltham, MA) for 45 min at 37°C.

For assessment of cellular co-localization of LS301 with lipid rafts, the Vybrant AlexaFluor 488 Lipid Raft Labeling Kit (Cat. No.: V34403, Thermo Fisher Scientific, Waltham, MA, USA) was used according to the manufacturer's instructions. Briefly, 4T1 cells were grown overnight in eight-chambered slides (Thermo-Fisher Scientific, Waltham, MA, USA) in phenol-free DMEM + 10% FBS. LS301 was added to 4T1 cells at 5μM for 1 h followed by staining with AlexaFluor 488-conjugated cholera toxin B for 10 min. at 4°C, washing with PBS, and followed by addition of anti-cholera toxin B antibody for 15 min. at 4°C to crosslink labeled lipid rafts and washing with PBS. Slides were mounted with Fluoromount-G mounting medium (Thermo-Fisher Scientific) prior to viewing. LS301 and AlexaFluor 488 fluorescence were imaged using the cypate filter set (Ex/Em 750-800 nm/818-873 nm) and FITC filter set (Ex/Em 460-500/510-560nm), respectively.

For live cell imaging of LS301 cell surface binding at 4ºC, at first, the tumour cells and fibroblast cells were incubated with 1μM of LS301 in culture medium for 1 h at 4ºC in 35 mm glass bottom culture dishes (MatTek Co., Ashland, MA, USA). In the 1.5 mL tubes, 1:250 monoclonal rabbit anti-ANXA2 antibody (Cell signaling Technology. Inc. Danvers, MA, USA) was incubated with 1:500 Alexa 488 anti-rabbit antibody (Thermo Fisher Scientific), and 1:250 mouse anti-pANXA2 antibody (Santa Cruz biotechnology, Inc. Santa Cruz, CA) was incubated with 1:500 Alexa 546 donkey anti-mouse antibody (Thermo Fisher Scientific, Waltham, MA, USA) for 1 h at 37 ºC respectively. Then, the cells treated with LS301 were washed twice and incubated with the first and second antibodies complexes for another 1 h at 4 ºC. Secondary antibody treatment alone served as controls. After washing twice, the cells were imaged using an FV1000 confocal microscope, and the mean fluorescence intensities (Ex/Em = 488/510-530 nm; Ex/Em = 546/555 – 600 nm, 633/645 −700 nm; Ex/Em = 780/805 – 830 nm) were determined using the FV1000 software.

For LS301 cell internalization studies involving insulin treatment, cells were grown on Lab-Tek slides overnight. HEK 293T cells (or in some cases 4T1 cells) were maintained in DMEM medium supplemented with 10% fetal bovine serum and 100 units/mL penicillin.

After DNA transfection, the HEK 293T$^{Anxa2\text{-}WT\text{-}GFP}$ and HEK 293T$^{Anxa2\text{-}Y23A\text{-}GFP}$ cells were maintained in DMEM medium with 500 μg/mL G418, 10% fetal bovine serum, and 100 units/mL penicillin. The medium was changed and cells were grown in serum-starved conditions overnight. Cells were then cultivated in the presence or absence of 100 nM insulin for 4 h. Then 1 μM of LS301 was added to each sample to incubated for 4 h or 24 h at 37°C. Cells were imaged using an FV1000 confocal microscope, and the mean fluorescence intensities (Ex/Em = 488/495 nm; Ex/Em = 590/617 nm; Ex/Em = 780/805 – 830 nm) were determined using the FV1000 software. For Western blot analysis of insulin/PP2-induced change in cellular pANXA2 levels, 4T1 cells were treated with insulin or PP2 as above, lysed, and subjected to SDS-PAGE analysis as described previously the Western Blot methods section.

For mechanistic LS301 cell internalization experiments with endocytosis pathway inhibitors, 4T1 murine breast cancer cells were seeded in an 8 well plate at a density of 5000 cells/well with DMEM media supplemented with 10% FBS and penicillin/streptomycin and incubated overnight at 37˚C. The next day, culture media was removed, followed by pre-treatment of cells with chlorpromazine hydrochloride at 13 μg/mL for 30 min, filipin complex at 3.2 μg/mL for 1 h, or amiloride hydrochloride at 300 μM for 1 h in 300 μL volume of cell culture media. Next, the drug-containing media was removed at the end of the incubation period and replaced with fresh culture media containing 6 μM or 0.9 μg/mL of LS301 in complete DMEM for 1 h at 37°C. For Pitstop 2 studies, 4T1 cells were incubated with Pitstop 2 reagent at 25μM for 20 minutes followed by incubation with LS301 at 2μM for 1 or 3 h. After LS301 treatment the culture media was removed followed by addition of culture media containing SYTO 17 nuclear dye for 40 min at 37°C. Finally the nuclear stain media was removed, cells washed 2 times with PBS and later re-suspended in culture media for live cell confocal microscopy imaging using Ex/Em = 780/805 – 830 nm for LS301 and Ex/Em = 621/634 nm for SYTO 17. ImageJ software was used to obtain the corrected total cell fluorescence (CTCF) value from multiple cells per condition and data summarized with a box plot. Background signal was maintained at zero background for the analysis.

For LS301 intracellular trafficking experiments, 4T1 cells were cultured overnight using similar parameters as above. The next day culture media was removed, followed by incubation of cells with 200 μL of 4 μM LS301 in complete culture media for 5 h at 37°C. At the end of this internalization process, LS301-containing media was removed followed by three PBS washes. Fluorescence organelle staining and imaging were performed according to manufacturers' protocols using VectaCell Rhodamine 123 for mitochondria, Lysotracker for lysosomes, BODIPY TR Ceramide for Golgi apparatus and CellLight Peroxisome-GFP, BacMam 2.0 for peroxisomes. Immunocytochemistry was performed with 4% paraformaldehyde fixation, permeabilization with 0.1% Triton X-100 solution and blocking with 5% normal goat serum and 1% BSA in 1X PBS blocking solution. Primary monoclonal antibodies against Rab5 (1:333) for early endosomes and Rab7 (1:333) for late endosomes were added to cells overnight at 4˚C. The next day, wells were washed three times in PBS and then incubated with secondary Ab (goat anti-rabbit Dylight 550 nm (1:500)) for 1 h. Finally wells were washed three times and then imaged without cover slipping with water immersion lens at 60x. ImageJ was used to perform co-localization analyses to obtain the Pearson's correlation coefficient (PCC) and the scatter plot inset.

For *in vitro* blocking studies of LS301, 4T1 luc/GFP cells were treated for 24 h with LS301 alone, blocking peptide LCKLSL plus LS301, scrambled blocking peptide LGKLSL plus LS301, or unlabeled LS301 analog LS637 plus LS301. Cells were prepared for confocal microscopy as described in Immunocytochemistry and Fluorescence Microscopy sections.

For co-culture experiments on intercellular pANXA2/ANXA2 transfer, fibroblasts (FB) (5×10^4 cells/well) were seeded on 35 mm glass bottom petri dish (MarTek Cor. Ashland, MA, USA) overnight prior to seeding of 5×10^4 of cancer cells and further culture overnight prior to the experiment. LS301 (1 μM) was incubated with co-cultures of FB and ANXA2-YFP transfected HL60 cells, co-cultures of FB and wild-type HL60 cells, or co-cultures of FB and 4T1-GFP cells at 37°C for 3 h and then washed twice with 0.01 M PBS (pH 7.4). Then, the cells were fixed with 4% paraformaldehyde for 10 min. For immunocytochemistry, slides were blocked with appropriate serum for 35 min or with 5% non-fat milk PBS (pH7.4) overnight at 4°C. Then, the slides were incubated with 1: 500 monoclonal rabbit anti-ANXA2 antibody (Cell signaling Technology. Inc. Danvers, MA, USA), 1: 500 monoclonal mouse anti-pANXA2 antibody (Santa Cruz biotechnology, Inc. Santa Cruz, CA, USA), and/or 1:250 monoclonal mouse anti-vimentin antibody (Santa Cruz Biotechnology, Santa Cruz, CA, USA) for 1 h at 37 °C. After washing twice with PBS, the tissue sections were incubated with 1:1000 Alexa 488 anti-rabbit antibody (Thermo Fisher Scientific, Waltham, MA) and/or 1: 1000 TRITC labeled donkey anti-mouse IgG in MPBS (Jackson ImmunoResearch Lab, West Grove, PA, USA), for 1 h at 25ºC. Finally, slides were imaged under confocal microscope as described in Fluorescence Microscopy methods section.

Fluorescence microscopy

Fluorescence microscopy was performed using either an Olympus FV1000 confocal microscope (Olympus Corp., Tokyo, Japan) with filters/channels as follows: Ex/Em = 488/510 – 530 nm; Ex/Em = 546/555 – 600 nm, 633/645-700 nm; Ex/Em =785 nm /805-830 nm; or epifluorescence microscope with filters/channels as follows: DAPI (Ex/Em = 330-385/420 nm), FITC (Ex/Em = 460-500/510-560 nm), Texas Red (Ex/Em = 542-582/604-644 nm), cypate (Ex/Em = 750-800/818-873 nm), using exposure times 1 to 30s and sensitivity settings ISO200-ISO1600, with the same parameters used for control and treatment groups unless otherwise indicated. ImageJ software (National Institutes of Health, Bethesda, MD, USA) was used for image processing.

Immunocytochemistry

In general, cells were fixed in Lab-Tek 8-chamber slides with 3% paraformaldehyde in PBS solution for 15 min. Nonspecific binding sites were blocked by PBS containing 10% normal donkey serum (blocking solution) for 1 h. Cells were incubated overnight at 4°C with the appropriate primary antibodies, after three 5 min PBS washes. Cells were then incubated at room temperature for 1 h with diluted secondary donkey anti-rabbit antibody (Alexa Fluor 594) in blocking solution. Slides were counterstained and mounted with cover slips for imaging on an FV1000 confocal microscope. Mean fluorescence intensities (Ex/Em = 590/617 nm) on the slide were determined using the FV1000 software.

Cell transfection and transduction

ANXA2-YFP expressing HL60 cells were generated by lentiviral transduction as follows. Human full-length ANXA2 cDNA in pCMV6-AC-GFP vector was purchased from OriGene Technologies (Rockville, MD, USA). BamHI, XhoI, and AgeI restriction enzymes and Quick Ligation kit were purchased from New England Biolabs (Ipswich, MA, USA). An FCIV lentiviral vector containing IRES-Venus YFP under the ubiquitin promoter was obtained as a generous gift from Dr. Mingjie Lee at the Hope Center, Washington University School of Medicine (St Louis, MO, USA). The ANXA2 cDNA was subcloned into the FCIV lentiviral vector by restriction digest of the ANXA2 cDNA vector with BamHI and XhoI enzymes, restriction digest of the FCIV vector with BamHI and AgeI enzymes, and ligation using Quick Ligation kit according to the manufacturer's instructions. Klenow fragment and dNTP nucleotide mix (New England Biolabs) were used to fill sticky ends.

HEK 293T cells (ATCC) were cultured overnight in Dulbecco's modified Eagle medium (DMEM) with 10% fetal bovine serum, 100 units/mL penicillin, and 100 μg/mL streptomycin prior to transfection. DNA constructs were transfected into HEK 293T cells using Genejuice (EMD Millipore, Burlington, MA) according to the manufacturer's instructions. Culture supernatants were collected 40 h after transfection, mixed 1:1 with Iscove's Modified Dulbecco's (IMDM) medium (Thermo Fisher Scientific) supplemented with 10% fetal bovine serum (FBS) and 1% Streptomycin, and added to HL60 cells in 6-well plates. At 72h post transduction, the HL60 cells were checked under confocal microscope for fluorescence. Populations of HL60 cells strongly expressing ANXA2-YFP were analyzed and collected by flow cytometry using a BD FACS AriaII Cell Sorter at a core laboratory at Washington University in St. Louis School of Medicine (St Louis, MO, USA). Cell viability was checked by luciferase MTS assay as described in the MTS Assay section of methods.

Transwell culture and extracellular vesicle transfer studies

For transwell studies, human dermal fibroblasts (300,000 cells/well) were cultured alone in 6 well plates or in transwell with 4T1 cells (100,000 cells/insert) suspended within transwell inserts (3 μm pore polycarbonate membrane, MilliporeSigma, St Louis, MO, USA). Cells were plated and grown in extracellular vesicle-depleted media for 72 h and subsequently stained for pANXA2 using rabbit anti-pANXA2 primary antibody (15 min. at 4°C) and donkey anti-rabbit AlexaFluor 594 conjugated secondary antibody (15 min. at 4°C) at 1:500 dilutions, and visualized by fluorescence microscopy using the Texas Red filter set (Ex/Em = 542-582/604-644 nm). Extracellular vesicle-depleted media was generated by collecting flow-through after centrifugal filtration of complete DMEM media using Amicon Ultra-100K (100 kDa molecular weight cutoff membrane) devices (MilliporeSigma, St Louis, MO). For extracellular vesicle transfer studies, supernatants from 4T1 cells cultured in extracellular vesicle-depleted media for 16 h were harvested and the 4T1-derived extracellular vesicle fraction was concentrated by serial centrifugal filtration on Amicon Ultra-100K devices as described above. The 4T1-derived extracellular vesicle fraction was then added to fibroblasts (60 μg/well) for 24 h, with untreated fibroblasts as control. LS301 was then added at 5 μM for 1 h and LS301 uptake was visualized by fluorescent microscopy using the cypate filter set (Ex/Em 750-800 nm/818-873 nm). A separate group of fibroblasts

with or without added 4T1-derived extracellular vesicles was stained for pANXA2 using rabbit anti-pANXA2 primary antibody and donkey anti-rabbit AlexaFluor 594 conjugated secondary antibody at 1:500 dilutions, and visualized by fluorescence microscopy as above.

MTS Assay

6,000 4T1 or fibroblast cells (n=3) were seeded in 96-well plates and cultured in DMEM with 10% FBS at 37°C overnight before treatment with different concentrations of LS301 for 48 hours or 72 hours. Cell viability was evaluated using CellTiterGlo Luminescent cell viability assay (Promega, USA) according to the manufacturer's instructions by standard plate reader for luminescence. The luminescence intensity from cells was normalized to reagent alone.

Apoptosis Analysis using FITC-conjugated Annexin V Apoptosis Detection kit

Overnight cultured 4T1 tumour cells in 96 well plates were treated with 0.5 μg/ml of DOX for 3 h as positive control. After treatment with different concentrations of LS301 for 48 h or 72 h, the cells were trypsinized, centrifuged and washed twice with PBS (pH 7.4) before cell cytometry. Apoptotic cell death was determined using FITC Annexin V Apoptosis Detection kit (Biolegend, USA) according to manufacturer's instructions. Data were acquired and analyzed using BD FACS AriaII Cell Sorter (Beckman Coulter, USA) at the core laboratory at Washington University in St. Louis School of Medicine.

Immunohistochemistry

In general, tissues of interest were harvested and frozen at −80°C in Optimal Cutting Temperature (OCT) media (storage at ≤−20°C). Frozen sections were cut at 10 μm thickness, and slides were stored at −40°C. LS301 fluorescence signal was then assessed by fluorescence microscopy using Cy7 filters or confocal microscope. Sections were subsequently fixed with 4% paraformaldehyde for 10 min. For immunohistochemistry, slides were blocked with appropriate serum for 35 min or with 5% non-fat milk PBS (pH7.4) overnight at 4 °C, and incubated with primary antibody overnight at 4°C or 1h at 37°C. For ANXA2/pANXA2 studies, tissue sections were incubated with 1: 250 monoclonal rabbit anti-ANXA2 antibody (Cell signaling Technology. Inc. Danvers, MA) or 1: 250 monoclonal mouse anti-pANXA2 antibody (Santa Cruz biotechnology, Inc. Santa Cruz, CA). After washing twice with PBS, the tissue sections were incubated with 1:1000 AlexaFluor 488 anti-rabbit antibody (Thermo Fisher Scientific, Waltham, MA) and 1: 800 TRITC labeled donkey anti-mouse IgG in MPBS (Jackson ImmunoResearch Lab, West Grove, PA, USA), for 1 h at 25 ºC respectively. Slides were washed again and stained with Hoechst or DAPI nuclear stains for 5 min or stained with 1:4000 nucleus dye ToPro3 (Thermo Fisher Scientific, Waltham, MA) for 45 min at 37°C. After final washes, a coverslip with aqueous fluorescence-saving mounting media was applied prior to imaging. Images were co-registered with others from the same sections to allow co-localization analysis.

For H&E staining, the same section or an adjacent frozen section was fixed for 10 min in 4% paraformaldehyde solution (Sigma, St. Louis, MO, USA) and stained with Harris hematoxylin for 90 seconds and with eosin (Sigma, St .Louis, MO) for 15 seconds, and then washed with tap water for 5 min. The tissue sections were mounted with Richard-Allan

Scientific mounting medium (Thermo Fisher Scientific) and cover slips for microscopic examination.

For Z-stack imaging, the frozen 4T1 tumour tissue sections (10 μm thickness) were warmed in PBS (pH 7.4) for 5 min, and then stained with SYTO-13 green fluorescent nuclear stain (Thermo Fisher Scientific, Waltham, MA) for 45 min at 37 ºC. Slides were imaged under confocal microscope at Ex/Em = 488/510-530 nm for SYTO-13 and Ex/Em = 780/805 – 830 nm for detection of LS301. Each step of the Z-stack imaging ranged from 0.8 μm to 1.6 μm.

Quantitative analysis of fluorescence in tissue sections

For quantitative correlation of pANXA2 expression to LS301 fluorescence in 4T1 luc-GFP, HT1080, and BxPC-3 tumours, the ImageJ plugin Co-localization Finder was applied to three representative tumour areas for each tumour type and used to determine Pearson's correlation coefficients for pANXA2/LS301 signal overlap. For quantitative analysis of pANXA2 or ANXA2 signal within human tissues, FV1000 software was applied to calculate the fluorescence intensity at different areas in tumour tissues (n=3 mice /group, n=15 view spots). Ten lines were drawn in each view site, three view sites were chosen in tissue sections using 10x and 60x objective lens to do quantitative analysis. All values are the mean + S.D. and Student's two –tailed unpaired t-test was used to compare the difference. $P < 0.05$ was accepted as statistically different. For quantitative analysis of intratumoral LS301 levels in 4T1 luc/GFP, HT1080, and BxPC-3 tumours, mean fluorescence was measured for six independent views including both peripheral and core tumour tissues for each tumour type using ImageJ software (Analysis>Measure function). For quantitation of intratumoral distribution (periphery vs. core) of LS301 in 4T1 luc/GFP tumours, mean fluorescence was measured for three independent views of peripheral tumour tissues versus three independent views of core tumour tissues using the ImageJ software as above.

In vivo probe distribution studies

To establish the various tumour models, nude, Balb/c, or C57BL/6 mice were injected with 10^5-10^7 tumour cells subcutaneously on unilateral or bilateral flanks. In select cases, spontaneous tumour models were used. Animals injected subcutaneously with saline served as sham tumour controls. For near-infrared imaging, 100 μL volumes of 60 μM LS301 or cypate in PBS were injected intravenously by lateral tail vein, and animals were imaged using a Pearl Small Animal Imager (LI-COR Biotechnology, Lincoln, NE, USA) at the indicated time points. Images were acquired using standard Pearl Small Animal Imager software acquisition settings (<30s scan time for 700, 800, and white channels; 85μm resolution; ex/em wavelengths for 700, 800, and white channels were 685nm/720nm, 785nm/820nm, and white/720nm, respectively). In some experiments, probes were formulated in 1% albumin in PBS. Animals were shaved using commercially available hair removal equipment and products prior to imaging. For experiments involving anaesthesia, animals were anesthetized with isoflurane (inhalation of 2% isoflurane vaporized in oxygen). For experiments requiring tissue analysis, mice were euthanized by cervical dislocation under isoflurane anesthesia. Organs were harvested by surgical dissection. For quantitative organ biodistribution studies, individual regions of interest were free-drawn

around each organ of interest and fluorescence was quantified using the Pearl Small Animal Imager software.

Flow cytometry and cell sorting

For flow cytometric analysis of cells from LS301-labeled 4T1 tumour xenografts, after injection of LS301 in 4T1 luc/GFP tumour-bearing mice at the time points indicated, the mice were imaged, euthanized, and tumours were excised and kept at −80°C prior to analysis. Tumours were thawed, cut into small pieces, and incubated in trypsin for 1 to 2 h at 37°C, and the tissue was dissociated and filtered with a 40-μm cell strainer tube (Falcon 352235) to collect the sample and washed with PBS (pH 7.4) three times and further centrifuged for collection. The cells were sorted using a BD FACS AriaII Cell Sorter at a core laboratory at Washington University in St. Louis School of Medicine (St Louis, MO, USA). Untreated cells, cells treated with LS301 (4 μM for 24h), wild-type 4T1 cells (without GFP), and 4T1 luc/GFP cells were used for compensation and gating. The sorted cells were classified and collected in fresh Iscove's Modified Dulbecco's medium (IMDM) supplemented with 10% fetal bovine serum (FBS) and 1% Streptomycin.

Fluorescence imaging guided surgical margin assessment

Three 6-week old Balb/c mice were implanted with 100,000 4T1-Luc/GFP murine breast cancer cells, orthotopically in the mammary fat pad below the right front leg. Seven to ten days post implantation, all three mice were injected with 100 μL of calcium-formulated LS301 (5mM Ca/60μM LS301) via tail vein injection. Twenty-four hours post-injection, these mice were subjected to image-guided surgery using the Cancer Vision Goggle (CVG) system that has been previously validated in human breast cancer patients for surgical guidance [51,52]. Mice were maintained under anaesthesia using continuous 2% isofluorane gas inhalation. A midline incision was made from the sternum to the base of the right front leg to create a skin flap along the tumour guided by LS301 fluorescence visualized using the CVG. The skin flap was deflected to expose and resect the tumour under fluorescence guidance. The surgical bed was surveyed for residual fluorescence and any additional fluorescent tissue identified using the CVG was resected. In vivo confirmatory closed-field fluorescence images were obtained using the Pearl small animal imaging system (Li-Cor Biosciences, Lincoln, NE, USA) to ensure no residual fluorescence was left behind. Additional in vivo validation of complete tumour resection was obtained using quantitative bioluminescence imaging using the IVIS imaging system (PerkinElmer, Waltham, MA, USA), after injecting the mice with luciferin intraperitoneally before start of surgical resection.

All resected tissues were embedded in Tissue-Tek OCT (Sakura Finetek, Torrance, CA, USA) and frozen for preservation. All preserved tissues were sectioned into 10 uM thick slices using a cryo-microtome and immediately mounted onto microscope slides. Consecutive tissue section slides were observed for LS301 fluorescence using the epifluorescence microscope (Olympus B61). These sections were then stained using hematoxylin and eosin to identify cancerous tissue and imaged under brightfield conditions using the epifluorescence microscope to find correspondence of the fluorescence and cancerous regions.

Fluorescence quantification of images obtained using the CVG were done using ImageJ software (NIH). Tumour-to-background ratio (TBR) calculations and statistical analyses were done using Origin Pro 8.0 software (OriginLabs). Means and standard errors were used to denote TBR average values and errors respectively. Paired student's t-tests were used to compare the TBRs before and after tumour resection as a measure of complete tumour resection and lack of residual fluorescence in the surgical bed. A p value < 0.05 was considered statistically significant.

In vivo LS301-doxorubicin drug conjugate therapy

Athymic nude mice (n=3 per group) were subcutaneously implanted with HT1080 human fibrosarcoma cells. Tumour growth was measured by caliper twice weekly. On days 8, 11, and 15 post tumour implantation, mice were intravenously injected with either control (no treatment), doxorubicin alone, or LS301-doxorubicin drug conjugate at a dose of 0.5 μmol/kg. Mice were euthanized when tumours reached 2 cm diameter in any direction. Survival was plotted using Kaplan-Meier curves and statistical significance was assessed by Logrank test of untreated control vs. LS301-doxorubicin treatment.

Statistics

Unless otherwise noted, differences between sample means were analysed by two-tailed unpaired t-test with $p<0.05$ denoting statistical significance and error bars denote standard error (standard deviation / square root of n). For replicate experiments, sample size was at least (n) = 3 for each experimental group, which is the minimum required for exploratory imaging studies because each animal can be used for repeat experiments and imaged longitudinally but only counted as one sample. Pearson's correlation coefficient, image quantification and analysis were calculated using the ImageJ software plugin Co-localization Finder. Statistical analyses were performed using Microsoft Excel (Microsoft Corp.) or Origin Pro 8.0 software (OriginLabs).

Data availability

All data generated and analysed during the study are available within the paper and its Supplementary Information, with the exception of the codes of company-proprietary imaging software.

Supplementary Material

Refer to Web version on PubMed Central for supplementary material.

Acknowledgements

This study was supported primarily by a research grant from the National Cancer Institute (R01 CA171651) and in part by grants from the National Institutes of Health (U54 CA199092, R01 EB021048, P50 CA094056, P30 CA091842, S10 OD016237, S10 RR031625, and S10 OD020129), the Department of Defense Breast Cancer Research Program (W81XWH-16-1-0286), and the Alvin J. Siteman Cancer Research Fund (11-FY16-01). We thank the Alvin J. Siteman Cancer Center at Washington University School of Medicine and Barnes-Jewish Hospital in St. Louis, MO, and the Institute of Clinical and Translational Sciences (ICTS) at Washington University in St. Louis, for the use of the Tissue Procurement Core which provided tissues of breast-cancer patients. The Siteman Cancer Center is supported in part by an NCI Cancer Center Support Grant P30 CA091842, and the ICTS is funded by the National Institutes of Health's NCATS Clinical and Translational Science Award (CTSA) program

grant UL1 TR002345. We thank Gabriel Birrane for providing the purified ANXA2 and pANXA2 protein reagents used in the initial study.

References

1. Lyssiotis CA & Kimmelman AC Metabolic Interactions in the Tumor Microenvironment. Trends Cell Biol 27, 863–875, doi:10.1016/j.tcb.2017.06.003 (2017). [PubMed: 28734735]
2. Dagogo-Jack I & Shaw AT Tumour heterogeneity and resistance to cancer therapies. Nat Rev Clin Oncol 15, 81–94, doi:10.1038/nrclinonc.2017.166 (2018). [PubMed: 29115304]
3. Krueger KE & Srivastava S Posttranslational protein modifications: current implications for cancer detection, prevention, and therapeutics. Mol Cell Proteomics 5, 1799–1810, doi:10.1074/mcp.R600009-MCP200 (2006). [PubMed: 16844681]
4. Pinho SS & Reis CA Glycosylation in cancer: mechanisms and clinical implications. Nat Rev Cancer 15, 540–555, doi:10.1038/nrc3982 (2015). [PubMed: 26289314]
5. Parker CE, Mocanu V, Mocanu M, Dicheva N & Warren MR in Neuroproteomics (ed Alzate O) (CRC Press/ Taylor & Francis, 2010).
6. Zhao Y & Jensen ON Modification-specific proteomics: strategies for characterization of post-translational modifications using enrichment techniques. Proteomics 9, 4632–4641, doi:10.1002/pmic.200900398 (2009). [PubMed: 19743430]
7. Olsen JV & Mann M Status of large-scale analysis of post-translational modifications by mass spectrometry. Mol Cell Proteomics 12, 3444–3452, doi:10.1074/mcp.O113.034181 (2013). [PubMed: 24187339]
8. Silva ML Cancer serum biomarkers based on aberrant post-translational modifications of glycoproteins: Clinical value and discovery strategies. Biochim Biophys Acta 1856, 165–177, doi:10.1016/j.bbcan.2015.07.002 (2015). [PubMed: 26232626]
9. Diaz-Fernandez A, Miranda-Castro R, de-Los-Santos-Alvarez N & Lobo-Castanon MJ Post-translational modifications in tumor biomarkers: the next challenge for aptamers? Anal Bioanal Chem 410, 2059–2065, doi:10.1007/s00216-018-0861-9 (2018). [PubMed: 29353432]
10. Bharadwaj A, Bydoun M, Holloway R & Waisman D Annexin A2 heterotetramer: structure and function. Int J Mol Sci 14, 6259–6305, doi:10.3390/ijms14036259 (2013). [PubMed: 23519104]
11. Lokman NA, Ween MP, Oehler MK & Ricciardelli C The role of annexin A2 in tumorigenesis and cancer progression. Cancer Microenviron 4, 199–208, doi:10.1007/s12307-011-0064-9 (2011). [PubMed: 21909879]
12. Mohammad HS et al. Annexin A2 expression and phosphorylation are up-regulated in hepatocellular carcinoma. Int J Oncol 33, 1157–1163 (2008). [PubMed: 19020748]
13. Diaz VM, Hurtado M, Thomson TM, Reventos J & Paciucci R Specific interaction of tissue-type plasminogen activator (t-PA) with annexin II on the membrane of pancreatic cancer cells activates plasminogen and promotes invasion in vitro. Gut 53, 993–1000 (2004). [PubMed: 15194650]
14. Mai J, Waisman DM & Sloane BF Cell surface complex of cathepsin B/annexin II tetramer in malignant progression. Biochim Biophys Acta 1477, 215–230 (2000). [PubMed: 10708859]
15. Sharma MR, Koltowski L, Ownbey RT, Tuszynski GP & Sharma MC Angiogenesis-associated protein annexin II in breast cancer: selective expression in invasive breast cancer and contribution to tumor invasion and progression. Exp Mol Pathol 81, 146–156, doi:10.1016/j.yexmp.2006.03.003 (2006). [PubMed: 16643892]
16. Shiozawa Y et al. Annexin II/annexin II receptor axis regulates adhesion, migration, homing, and growth of prostate cancer. J Cell Biochem 105, 370–380, doi:10.1002/jcb.21835 (2008). [PubMed: 18636554]
17. Jaiswal JK et al. S100A11 is required for efficient plasma membrane repair and survival of invasive cancer cells. Nat Commun 5, 3795, doi:10.1038/ncomms4795 (2014). [PubMed: 24806074]
18. Deora AB, Kreitzer G, Jacovina AT & Hajjar KA An annexin 2 phosphorylation switch mediates p11-dependent translocation of annexin 2 to the cell surface. J Biol Chem 279, 43411–43418, doi:10.1074/jbc.M408078200 (2004). [PubMed: 15302870]

19. Zheng L et al. Tyrosine 23 phosphorylation-dependent cell-surface localization of annexin A2 is required for invasion and metastases of pancreatic cancer. PLoS One 6, e19390, doi:10.1371/journal.pone.0019390 (2011). [PubMed: 21572519]
20. de Graauw M et al. Annexin A2 phosphorylation mediates cell scattering and branching morphogenesis via cofilin Activation. Mol Cell Biol 28, 1029–1040, doi:10.1128/MCB.01247-07 (2008). [PubMed: 18070928]
21. Rescher U, Ludwig C, Konietzko V, Kharitonenkov A & Gerke V Tyrosine phosphorylation of annexin A2 regulates Rho-mediated actin rearrangement and cell adhesion. J Cell Sci 121, 2177–2185, doi:10.1242/jcs.028415 (2008). [PubMed: 18565825]
22. Wang YQ et al. Tyrosine 23 Phosphorylation of Annexin A2 Promotes Proliferation, Invasion, and Stat3 Phosphorylation in the Nucleus of Human Breast Cancer SK-BR-3 Cells. Cancer Biol Med 9, 248–253, doi:10.7497/j.issn.2095-3941.2012.04.005 (2012). [PubMed: 23691485]
23. Phipps KD, Surette AP, O'Connell PA & Waisman DM Plasminogen receptor S100A10 is essential for the migration of tumor-promoting macrophages into tumor sites. Cancer Res 71, 6676–6683, doi:10.1158/0008-5472.CAN-11-1748 (2011). [PubMed: 22042827]
24. Achilefu S et al. Synergistic effects of light-emitting probes and peptides for targeting and monitoring integrin expression. Proc Natl Acad Sci U S A 102, 7976–7981, doi:10.1073/pnas.0503500102 (2005). [PubMed: 15911748]
25. Bloch S et al. Targeting Beta-3 integrin using a linear hexapeptide labeled with a near-infrared fluorescent molecular probe. Mol Pharm 3, 539–549, doi:10.1021/mp0600642 (2006). [PubMed: 17009853]
26. Liu T et al. Enhancing protein stability with extended disulfide bonds. Proc Natl Acad Sci U S A 113, 5910–5915, doi:10.1073/pnas.1605363113 (2016). [PubMed: 27162342]
27. Achilefu S, Dorshow RB, Bugaj JE & Rajagopalan R Novel receptor-targeted fluorescent contrast agents for in vivo tumor imaging. Investigative radiology 35, 479–485 (2000). [PubMed: 10946975]
28. Berezin MY et al. Rational approach to select small peptide molecular probes labeled with fluorescent cyanine dyes for in vivo optical imaging. Biochemistry 50, 2691–2700, doi:10.1021/bi2000966 (2011). [PubMed: 21329363]
29. Goiffon RJ, Akers WJ, Berezin MY, Lee H & Achilefu S Dynamic noninvasive monitoring of renal function in vivo by fluorescence lifetime imaging. J Biomed Opt 14, 020501, doi:10.1117/1.3095800 (2009). [PubMed: 19405707]
30. Thota R, Pauff JM & Berlin JD Treatment of metastatic pancreatic adenocarcinoma: a review. Oncology (Williston Park) 28, 70–74 (2014). [PubMed: 24683721]
31. Al-Hajeili M, Azmi AS & Choi M Nab-paclitaxel: potential for the treatment of advanced pancreatic cancer. Onco Targets Ther 7, 187–192, doi:10.2147/OTT.S40705 (2014). [PubMed: 24523592]
32. Kratz F Albumin as a drug carrier: design of prodrugs, drug conjugates and nanoparticles. J Control Release 132, 171–183, doi:10.1016/j.jconrel.2008.05.010 (2008). [PubMed: 18582981]
33. Valapala M & Vishwanatha JK Lipid raft endocytosis and exosomal transport facilitate extracellular trafficking of annexin A2. J Biol Chem 286, 30911–30925, doi:10.1074/jbc.M111.271155 (2011). [PubMed: 21737841]
34. Lippok S et al. Direct detection of antibody concentration and affinity in human serum using microscale thermophoresis. Anal Chem 84, 3523–3530, doi:10.1021/ac202923j (2012). [PubMed: 22397688]
35. Wienken CJ, Baaske P, Rothbauer U, Braun D & Duhr S Protein-binding assays in biological liquids using microscale thermophoresis. Nat Commun 1, 100, doi:10.1038/ncomms1093 (2010). [PubMed: 20981028]
36. Marks HL, Pishko MV, Jackson GW & Cote GL Rational design of a bisphenol A aptamer selective surface-enhanced Raman scattering nanoprobe. Anal Chem 86, 11614–11619, doi:10.1021/ac502541v (2014). [PubMed: 25329684]
37. Jung YS et al. Src family kinase inhibitor PP2 enhances differentiation of acute promyelocytic leukemia cell line induced by combination of all-trans-retinoic acid and arsenic trioxide. Leuk Res 38, 977–982, doi:10.1016/j.leukres.2014.05.019 (2014). [PubMed: 24953245]

38. Olwill SA, McGlynn H, Gilmore WS & Alexander HD Annexin II cell surface and mRNA expression in human acute myeloid leukaemia cell lines. Thromb Res 115, 109–114, doi:10.1016/j.thromres.2004.07.014 (2005). [PubMed: 15567461]
39. Hajjar KA et al. Tissue plasminogen activator binding to the annexin II tail domain. Direct modulation by homocysteine. J Biol Chem 273, 9987–9993 (1998). [PubMed: 9545344]
40. Lin EY et al. Progression to malignancy in the polyoma middle T oncoprotein mouse breast cancer model provides a reliable model for human diseases. Am J Pathol 163, 2113–2126, doi:10.1016/S0002-9440(10)63568-7 (2003). [PubMed: 14578209]
41. Fantozzi A & Christofori G Mouse models of breast cancer metastasis. Breast Cancer Res 8, 212, doi:10.1186/bcr1530 (2006). [PubMed: 16887003]
42. Dobrolecki LE et al. Patient-derived xenograft (PDX) models in basic and translational breast cancer research. Cancer Metastasis Rev 35, 547–573, doi:10.1007/s10555-016-9653-x (2016). [PubMed: 28025748]
43. Kazami T et al. Nuclear accumulation of annexin A2 contributes to chromosomal instability by coilin-mediated centromere damage. Oncogene 34, 4177–4189, doi:10.1038/onc.2014.345 (2015). [PubMed: 25347736]
44. LeBleu VS & Kalluri R A peek into cancer-associated fibroblasts: origins, functions and translational impact. Dis Model Mech 11, doi:10.1242/dmm.029447 (2018).
45. Hermann A, Donato R, Weiger TM & Chazin WJ S100 Calcium Binding Proteins and Ion Channels. Frontiers in Pharmacology 3, doi:10.3389/fphar.2012.00067 (2012).
46. Miele E, Spinelli GP, Miele E, Tomao F & Tomao S Albumin-bound formulation of paclitaxel (Abraxane ABI-007) in the treatment of breast cancer. Int J Nanomedicine 4, 99–105 (2009). [PubMed: 19516888]
47. Green MR et al. Abraxane, a novel Cremophor-free, albumin-bound particle form of paclitaxel for the treatment of advanced non-small-cell lung cancer. Ann Oncol 17, 1263–1268, doi:10.1093/annonc/mdl104 (2006). [PubMed: 16740598]
48. Komiya K et al. SPARC is a possible predictive marker for albumin-bound paclitaxel in non-small-cell lung cancer. Onco Targets Ther 9, 6663–6668, doi:10.2147/OTT.S114492 (2016). [PubMed: 27822069]
49. Frei E Albumin binding ligands and albumin conjugate uptake by cancer cells. Diabetol Metab Syndr 3, 11, doi:10.1186/1758-5996-3-11 (2011). [PubMed: 21676260]
50. Merlot AM, Kalinowski DS & Richardson DR Unraveling the mysteries of serum albumin-more than just a serum protein. Front Physiol 5, 299, doi:10.3389/fphys.2014.00299 (2014). [PubMed: 25161624]
51. Mondal SB et al. Optical See-Through Cancer Vision Goggles Enable Direct Patient Visualization and Real-Time Fluorescence-Guided Oncologic Surgery. Ann Surg Oncol 24, 1897–1903, doi:10.1245/s10434-017-5804-8 (2017). [PubMed: 28213790]
52. Liu Y et al. Hands-free, wireless goggles for near-infrared fluorescence and real-time image-guided surgery. Surgery 149, 689–698, doi:10.1016/j.surg.2011.02.007 (2011). [PubMed: 21496565]
53. Vanneman M & Dranoff G Combining immunotherapy and targeted therapies in cancer treatment. Nat Rev Cancer 12, 237–251, doi:10.1038/nrc3237 (2012). [PubMed: 22437869]
54. Baudino TA Targeted Cancer Therapy: The Next Generation of Cancer Treatment. Curr Drug Discov Technol 12, 3–20 (2015). [PubMed: 26033233]
55. Ecsedi P et al. Regulation of the Equilibrium between Closed and Open Conformations of Annexin A2 by N-Terminal Phosphorylation and S100A4-Binding. Structure 25, 1195–1207 e1195, doi:10.1016/j.str.2017.06.001 (2017). [PubMed: 28669632]
56. Achilefu S et al. Synthesis, in vitro receptor binding, and in vivo evaluation of fluorescein and carbocyanine peptide-based optical contrast agents. J Med Chem 45, 2003–2015 (2002). [PubMed: 11985468]
57. Seidel SA et al. Microscale thermophoresis quantifies biomolecular interactions under previously challenging conditions. Methods 59, 301–315, doi:10.1016/j.ymeth.2012.12.005 (2013). [PubMed: 23270813]

58. Garcia-Bonete MJ et al. Bayesian Analysis of MicroScale Thermophoresis Data to Quantify Affinity of Protein:Protein Interactions with Human Survivin. Sci Rep 7, 16816, doi:10.1038/s41598-017-17071-0 (2017). [PubMed: 29196723]

59. Jerabek-Willemsen M, Wienken CJ, Braun D, Baaske P & Duhr S Molecular interaction studies using microscale thermophoresis. Assay Drug Dev Technol 9, 342–353, doi:10.1089/adt.2011.0380 (2011). [PubMed: 21812660]

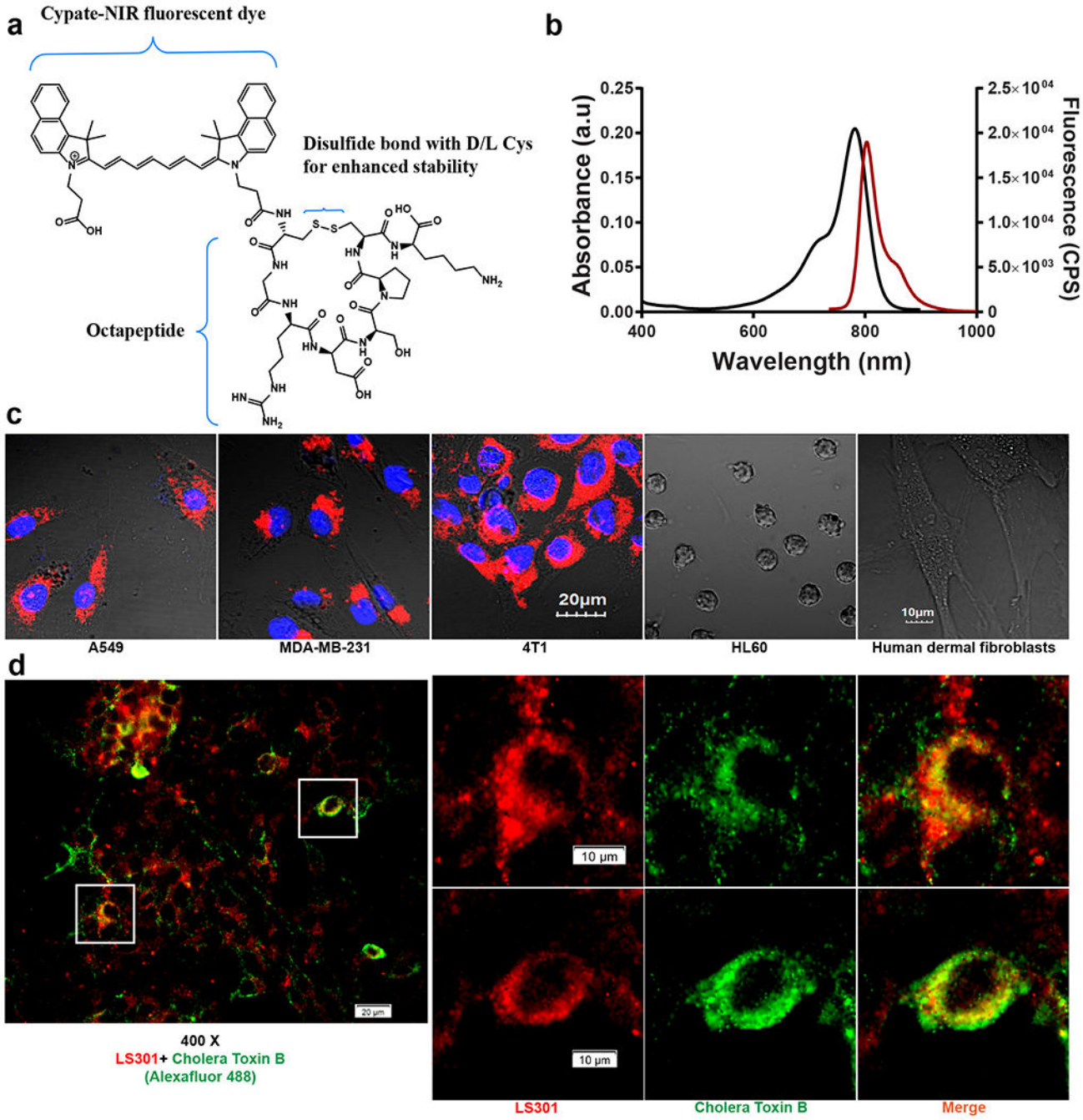

Figure 1 |. LS301 structure and cellular uptake.

(**a**) Chemical structure of LS301 and its components. (**b**) Spectral properties of LS301 used for cellular, whole-body, and tissue imaging. The black line indicates the absorption spectrum; the red line indicates the emission spectrum. (**c**) Representative images of LS301 internalization in different solid cancer cell lines or control (hematologic cancer or normal fibroblast) cell lines at 24 h post-incubation (n=3; see Supplementary Fig. 30a for additional images). Red indicates LS301 fluorescence; blue indicates SYTO-13 nuclear stain. **(d)** Representative 400x (left) and enlarged (right) fluorescence microscopy images of LS301

(red), cholera toxin B-AlexaFluor 488 conjugate (green, lipid raft labelling reagent), and overlay in 4T1 breast carcinoma cells (n=3; see Supplementary Fig. 30b for additional images). Cells were incubated with LS301 (5μM) for 1 h, followed by incubation with cholera toxin B-AlexaFluor 488 conjugate and anti-cholera toxin B antibody crosslinking prior to imaging. Scale bars for zoomed images are approximate.

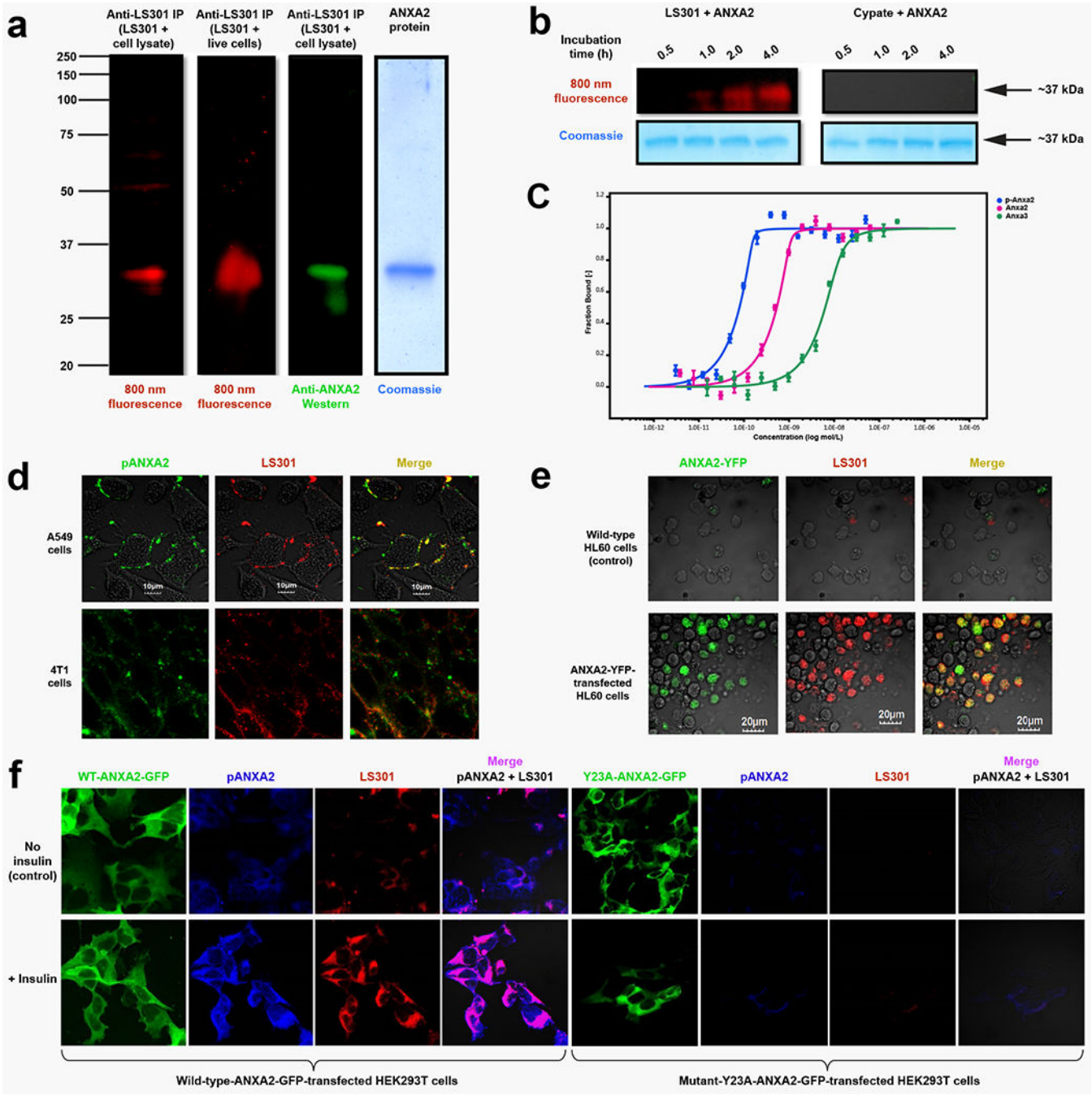

Figure 2 |. Identification of pANXA2 as a molecular target of LS301.

(**a**) Gel electrophoresis results showing (from left to right): LS301-associated proteins isolated by LS301 treatment of 4T1 cell lysates followed by immunoprecipitation (IP) with anti-LS301 antibody; LS301-associated proteins isolated by LS301 treatment of live 4T1 cells followed by cell lysis and immunoprecipitation with anti-LS301 antibody; anti-ANXA2 Western blot analysis of protein from LS301-cell lysate mixtures immunoprecipitated with anti-LS301 antibody; and Coomassie stain of purified ANXA2 protein. (**b**) Gel electrophoresis result on the in vitro binding of ANXA2 to LS301 (left) or

cypate (right; control fluorescent molecule), assessed by fluorescence. LS301 (10 μM) or cypate (10 μM) were incubated with 1 μg ANXA2 protein for the indicated times and subjected to 12% SDS-PAGE analysis. The Pearl imaging system was used for fluorescence imaging of gels. Red denotes LS301 or cypate fluorescence. For full length gel, see Supplementary Fig. 29. (**c**) MST analysis of binding affinities of LS301 to pANXA2, ANXA2, or ANXA3 (control). (**d**) Assessment of spatial co-localization between pANXA2 and LS301 in cancer cells by fluorescence microscopy and ICC after 1h incubation with LS301 at 4°C. (**e**) Assessment of LS301 uptake in wild-type ANXA2-negative HL60 cells vs ANXA2-YFP-transfected HL60 cells. (**f**) Correlation of cellular LS301 uptake with pANXA2 expression in HEK293T cells transfected with either phosphorylation-permissive wild-type-ANXA2-GFP (left) or phosphorylation-defective mutant-Y23A-ANXA2-GFP (right), as assessed by fluorescence microscopy and ICC after 24h incubation with LS301.

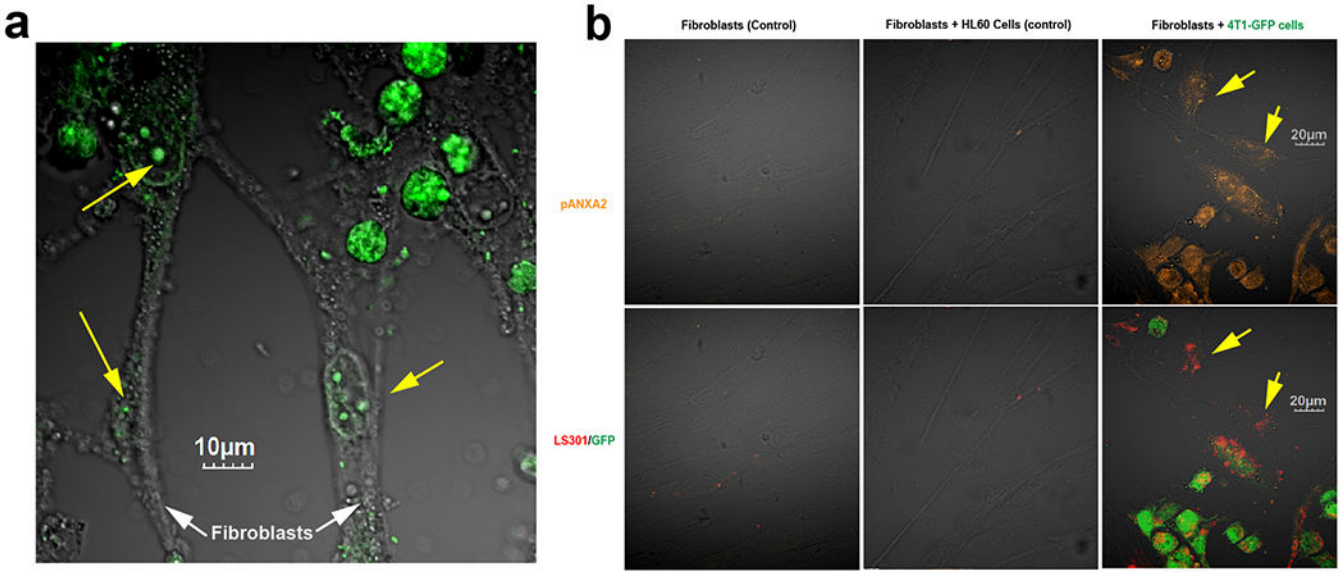

Figure 3 |. Intercellular spread of pANXA2 from cancer cells to fibroblasts.

(**a**) Representative fluorescence microscopy image depicting transfer of fluorescence from ANXA2-YFP-transfected HL60 cells to fibroblasts in co-culture (n=3; see Supplementary Fig. 30c for additional images). Green indicates GFP fluorescence. Yellow arrows in (a) denote examples of intercellularly transferred ANXA2. (**b**) Images depicting cellular pANXA2 expression and LS301 uptake in fibroblasts alone (top row), fibroblasts co-cultured with ANXA2-negative HL60 cells (middle row), or fibroblasts co-cultured with ANXA2-positive 4T1-GFP cells (bottom row), assessed by fluorescence microscopy and immunocytochemistry. Yellow arrows in (b) denote fibroblasts which were recipients of intercellular pANXA2 transfer (n=3).

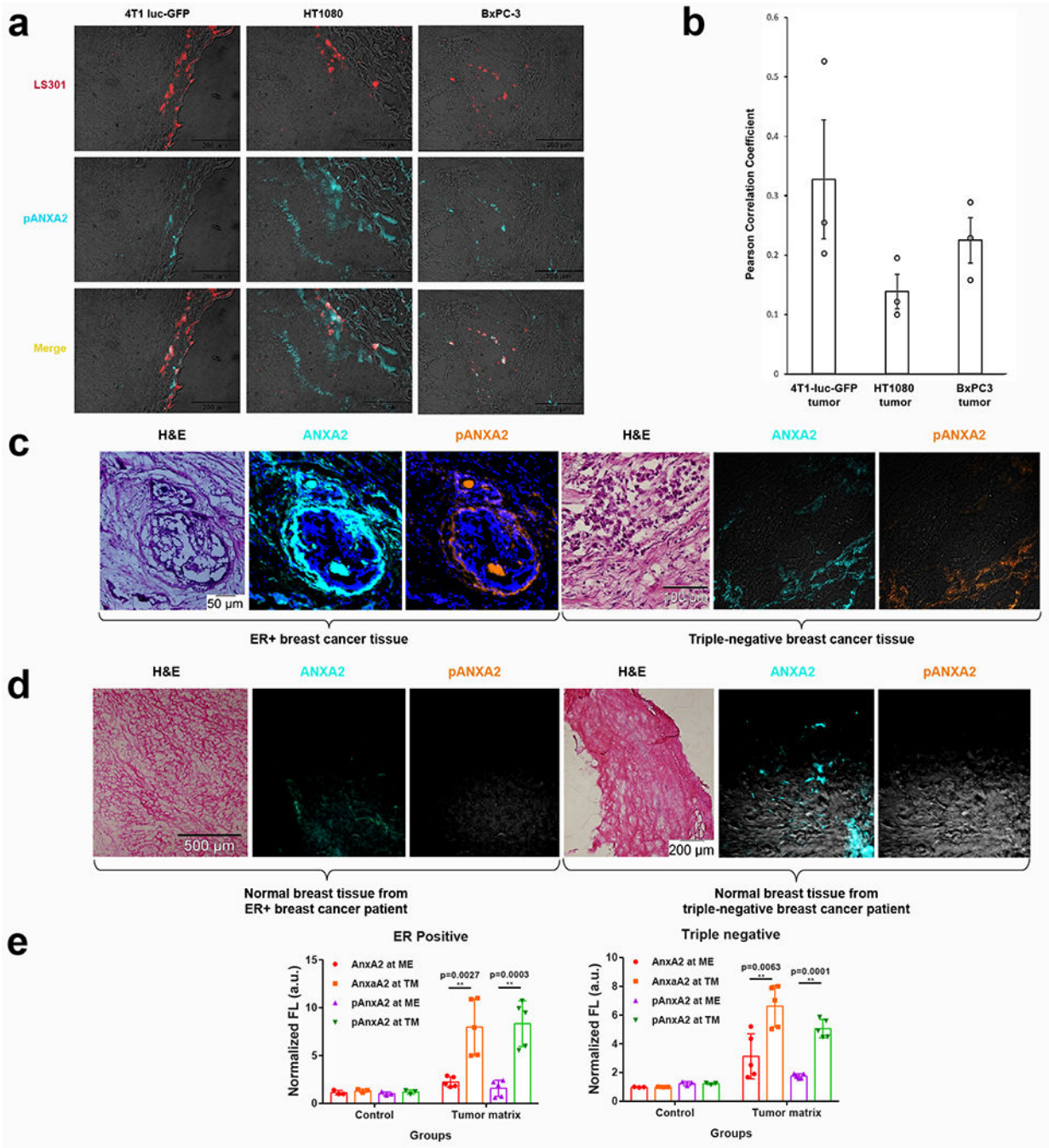

Figure 4 |. Expression of pANXA2 in solid cancer tissues.

(**a**) Immunohistochemistry (IHC) analysis of pANXA2 and ANXA2 expression in various cancer tissues derived from 4T1 luc-GFP, HT1080, and BxPC-3 murine tumours. (**b**) Quantitation of LS301-pANXA2 overlap. Three representative independent views from each tumour type were analyzed by the co-localization algorithm for LS301-pANXA2 signal correlation using ImageJ software. Error bars represent SE with n=3. (**c**) IHC analysis of ANXA2 and pANXA2 expression in breast cancer tissues from ER+ breast cancer patients (left) or triple-negative breast cancer patients (right). (**d**) IHC analysis of ANXA2 and

pANXA2 expression in normal breast tissues from ER+ breast cancer patients (left) or triple-negative breast cancer patients (right). (**e**) Quantitative assessment of ANXA2 and pANXA2 expression levels by fluorescence in ER-positive (left) or triple-negative (right) breast tumours relative to control noncancerous breast tissue. Control noncancerous breast tissues (n= 3) and breast tissue sections from malignant triple-negative (n=5) and ER-positive (n=5) breast cancer patients were used for quantitation. Ten ROIs were drawn in each view site, with three view sites chosen per tissue section for analysis. Means were compared using two-tailed t-test and error bars represent SE. ME = tumour microenvironment (connective tissue); TM = tumour matrix; FI = fluorescence intensity.

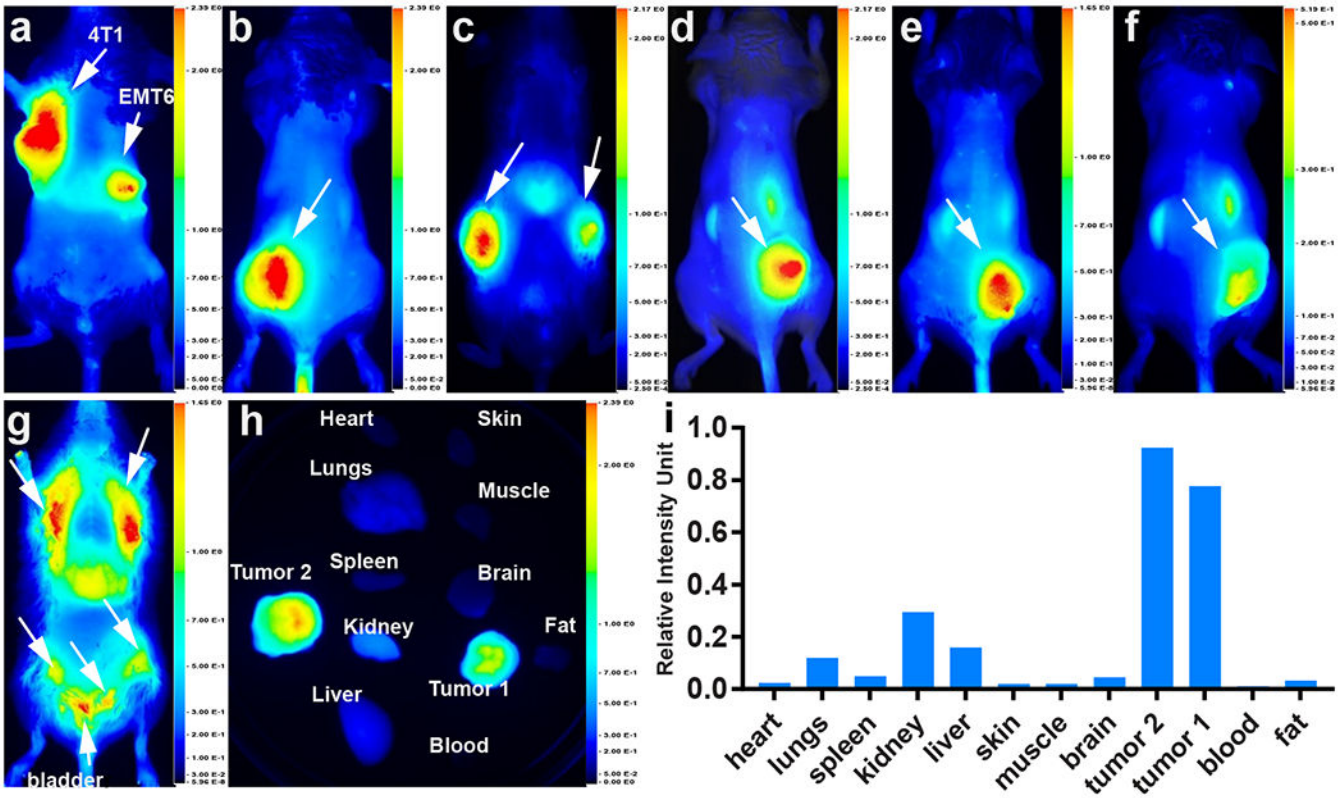

Figure 5 |. Selective accumulation of LS301 in diverse tumour models.

Uptake of LS301 in diverse primary (a-f) and metastatic (g) tumours as assessed by *in vivo* near infrared imaging 24h or more after LS301 administration. Arrows denote tumour locations. Results in (a-g) are representative of at least three independent experiments (n=3). (**a**) 4T1 mammary tumour (orthotopic) and EMT6 mammary carcinoma. (**b**) 4T1 mammary tumour (subcutaneous). (**c**) Patient-derived breast cancer xenograft. (**d**) HT1080 fibrosarcoma. (**e**) BXPC-3 pancreatic adenocarcinoma. (**f**) DBT brain gliobastoma. (**g**) MMTV-PyMT spontaneous breast cancer. (**h**) Typical *ex vivo* biodistribution of representative organs post LS301 injection (n=3; additional data in Supplementary Fig. 13c). (**i**) *Ex vivo* quantitation of (h) based on relative average fluorescence intensity per organ.

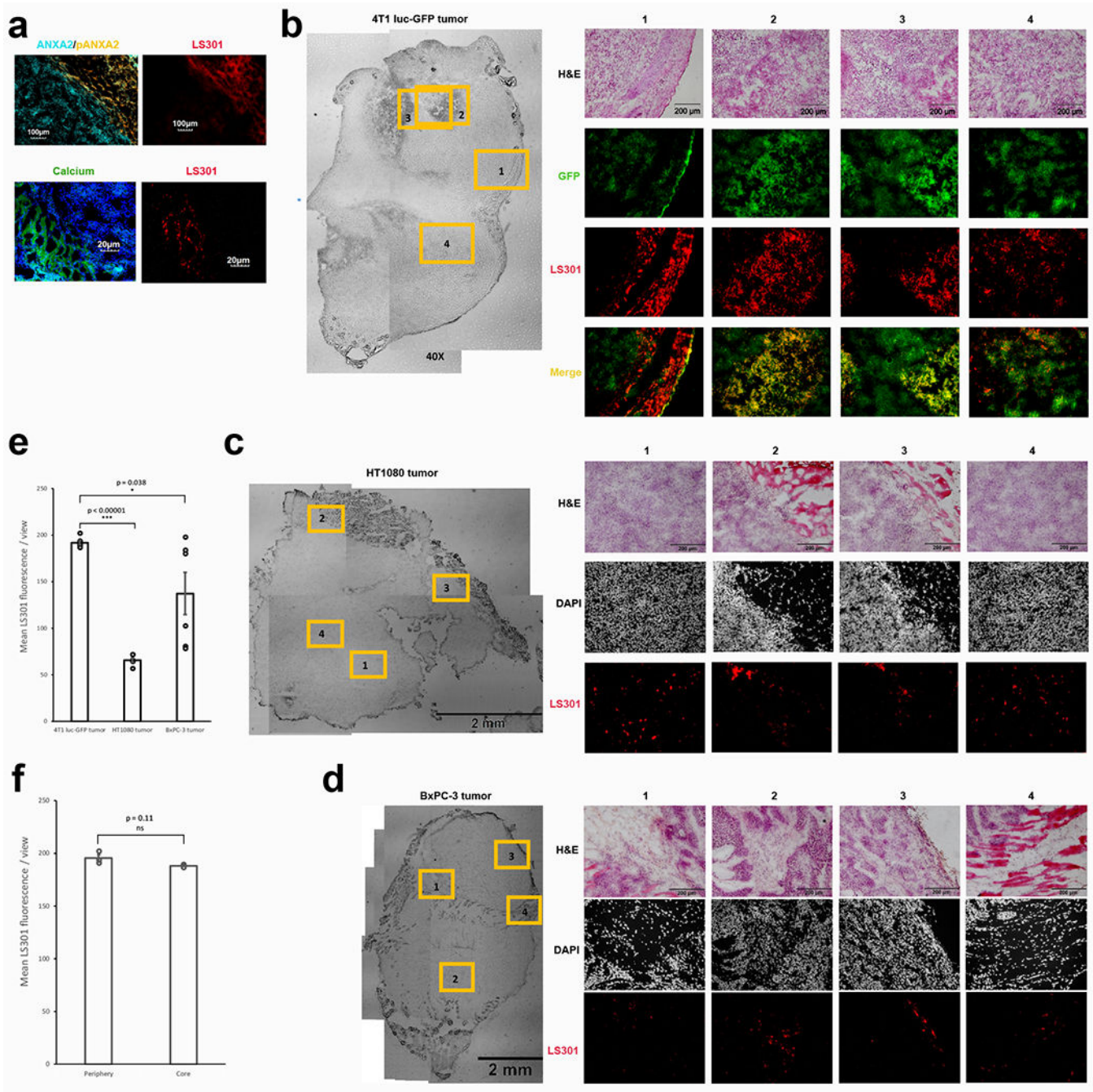

Figure 6 |. Intratumoral distribution of LS301 and co-localization of LS301 with pANXA2 and calcium.

(**a**) Representative IHC analysis of ANXA2 (cyan)/pANXA2 (yellow) vs. LS301 (red) distribution in 4T1 tumour sections (left); representative IHC analysis of calcium (green) and LS301 (red) distribution in HT-29 tumour sections (n=3; additional images in Supplementary Fig. 30d). Blue represents DAPI staining. (**b**) Representative IHC analysis of LS301 distribution in various regions of a subcutaneous 4T1 luc-GFP breast carcinoma tumour 24h after in vivo LS301 administration. Green denotes GFP fluorescence from 4T1-GFP cells; red denotes near-infrared fluorescence from LS301; yellow denotes overlap (n=3;

additional images in Supplementary Fig 20d and Supplementary Fig. 30e,f). (**c**) IHC analysis of LS301 distribution in various regions of a subcutaneous HT1080 fibrosarcoma tumour 24h after in vivo LS301 administration. Red denotes near-infrared fluorescence from LS301. (**d**) IHC analysis of LS301 distribution in various regions of a subcutaneous BxPC-3 pancreatic tumour 24h after in vivo LS301 administration. Red denotes near-infrared fluorescence from LS301. (**e**) Quantitative comparison of intratumoral LS301 levels among different tumours. Mean fluorescence was measured for six independent views including both peripheral and core tumour tissues for each tumour type using ImageJ software. Means were compared using two-tailed t-test and error bars represent SE with n=6. (**f**) Quantitative comparison of peripheral vs. core intratumoral distribution of LS301 within 4T1 tumours. Mean fluorescence was measured for three independent views of peripheral tumour tissues and three independent views of core tumour tissues using ImageJ software. Error bars represent S.E. with n=3.

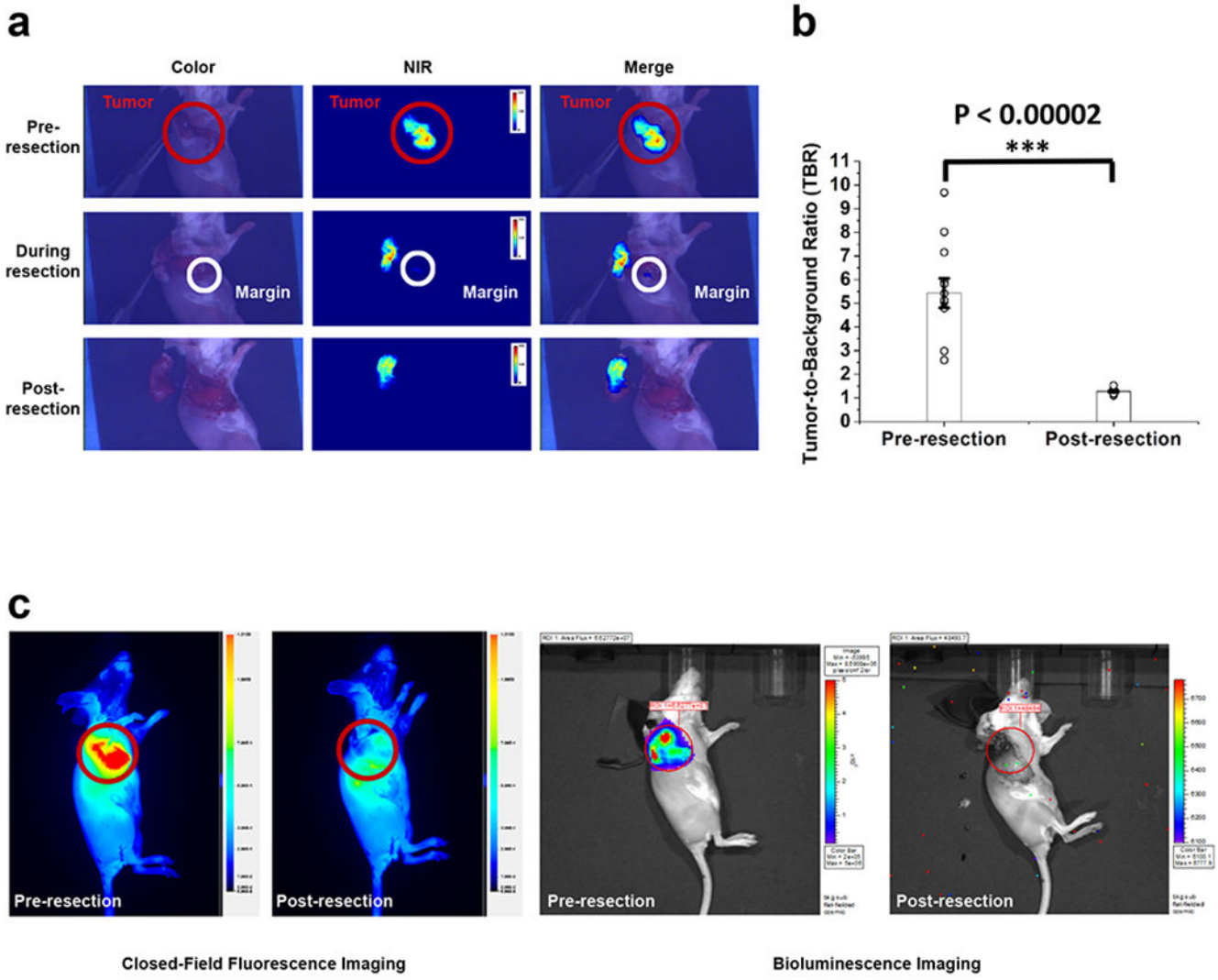

Figure 7 |. Intraoperative surgical guidance using the cancer vision goggle (CVG) system.
(**a**) Visualization of LS301 fluorescence showing exposed tumour before, during and after resection (left panel), showing bright LS301 fluorescence in the tumour (red circle), residual tumour detected (white circle) and resected tumour and tumour cavity with no residual fluorescence. (**b**) The tumour-to-background ratios (TBRs) for all three mice show a statistically significant decrease after fluorescence-guided resection indicating complete tumour removal. Tumour-to-background ratios were calculated using pre-resection and post-resection images, with 6 (n=6) or 3 (n=3) measurements per mouse for a total of 12 measurements. Means were compared using paired sample t test and error bars represent SE. (**c**) Confirmatory in vivo imaging using closed-field fluorescence imaging using Pearl small animal imaging system (left panel), showing tumour before resection and tumour cavity post resection with no significant residual fluorescence after CVG-LS301 guided tumour resection. Quantitative bioluminescence imaging (right panel) confirms all cancerous tissue was removed after resection compared to pre-resection image.